Comprehensive constraints on dark radiation injection after BBN

Alexander C. Sobotka,[1,*] Adrienne L. Erickcek,[1,†] and Tristan L. Smith[2,‡]
[1]*Department of Physics and Astronomy, University of North Carolina at Chapel Hill, Phillips Hall CB3255, Chapel Hill, North Carolina 27599, USA*
[2]*Department of Physics and Astronomy, Swarthmore College, Swarthmore, Pennsylvania 19081, USA*

(Received 8 January 2024; accepted 29 February 2024; published 26 March 2024)

We derive constraints on the injection of free-streaming dark radiation after big bang nucleosynthesis by considering the decay of a massive hidden sector particle into dark radiation. Such a scenario has the potential to alleviate the Hubble tension by introducing a new energy component to the evolution of the early Universe. We employ observations of the cosmic microwave background (CMB) from *Planck* 2018 and South Pole Telescope 2018, measurements of the primordial deuterium abundance, Pantheon+ type Ia supernovae data, and baryon acoustic oscillation measurements from BOSS DR12 to constrain these decay scenarios. Prerecombination decays are primarily restricted by observations of the CMB via their impact on the effective number of relativistic species. On the other hand, long-lived decay scenarios in which the massive particle lifetime extends past recombination tend to decrease the late-time matter density inferred from the CMB and are thus subject to constraints from Pantheon+ and baryon acoustic oscillations. We find that, when marginalizing over lifetimes of $\tau_Y = [10^{-12.08}, 10^{-1.49}]$ Gyr, the decaying particle is limited at 2σ to only contribute a maximum of 3% of the energy density of the Universe. With limits on these decays being so stringent, neither short-lived nor long-lived scenarios are successful at substantially mitigating the Hubble tension.

DOI: 10.1103/PhysRevD.109.063538

I. INTRODUCTION

Measurements of cosmological parameters from observations of the cosmic microwave background (CMB) [1], baryon acoustic oscillations (BAO) [2,3], and weak lensing [4,5] have become significantly more precise with time. However, this increased precision has introduced apparent discrepancies between local measurements of the Hubble constant (H_0) [6–9] and matter fluctuation parameter (S_8) [4,5,10] and the values predicted by the standard ΛCDM model based on observations of the CMB [1]. Many systematic uncertainties have been ruled out as the cause for these tensions [11–17], which persist across multiple probes, potentially hinting at the need for a new cosmological model.

Since the tension in H_0 can be recast as a tension in the measurement of the sound horizon at recombination [14], it is common for extensions of ΛCDM to introduce new contributions to the energy density of the Universe prior to recombination, thereby reducing the size of the sound horizon (e.g. [18–21]). One of the simplest extensions to ΛCDM that reduces the size of the sound horizon is the addition of free-streaming massless relics that alter the effective number of relativistic species, $N_{\rm eff}$ [19,22,23]. However, scenarios with a nonstandard $N_{\rm eff}$ during big bang nucleosynthesis (BBN) alter the abundance of primordial elements by changing the expansion rate during BBN and are therefore limited by measurements of primordial abundances of deuterium and helium [24–27]. Augmenting the radiation energy density *after* BBN (e.g. [28]) can bypass these limits, but there still exist stringent constraints on $N_{\rm eff}$ from the CMB alone [1,29–31]. Scenarios that alter $N_{\rm eff}$ after recombination by transferring energy from matter to radiation are also capable of increasing the value of H_0 inferred from the CMB by changing the angular diameter distance to the CMB [32–34].

In this work, we consider a massive hidden sector particle, which we call the Y particle, that decays solely into dark radiation (DR) after BBN. We place bounds on the particle decay rate (Γ_Y) as well as the maximum contribution that the particle makes to the energy density of the Universe. As in Sobotka *et al.* [35], we assume the hidden sector to be sufficiently cold such that the Y particle is nonrelativistic throughout BBN. The injected DR is assumed to be relativistic and free-streaming.

We only investigate decays into DR because scenarios that include decays into photons are significantly constrained [35]. Photon injection after BBN is constrained by its influence on primordial light-element abundances, with the most stringent bounds being placed on injected photons

*asobotka@live.unc.edu
†erickcek@physics.unc.edu
‡tsmith2@swarthmore.edu

with high enough energies to photodisintegrate primordial deuterium [36–42]. Even for injected photons that do not have enough energy to photodisintegrate deuterium, measurements of the abundance of deuterium still provide strict constraints via changes in the baryon-to-photon ratio during BBN [35]. Furthermore, the injection of new photons after a redshift of $z \sim 10^6$ results in spectral distortions of the CMB energy spectrum, so bounds on spectral distortions from the COBE satellite [43,44] or future measurements of the CMB spectrum [45] can be used to place limits on the time of photon injection [46–48]. In Sobotka *et al.* [35], we found that COBE constraints on spectral distortions required the Y particle lifetime to be less than ∼0.032 yr if more than ∼66% of the Y particle's energy was transferred to photons during its decay. Scenarios that do not inject photons are not subject to these constraints from BBN or spectral distortions and thus it is possible for the Y particle to decay much later, even after recombination.

Y particle decays into DR affect the CMB anisotropies and predicted abundance of primordial elements. The primary effect that an injection of DR prior to recombination has on the CMB anisotropies is via changes in $N_{\rm eff}$. Additionally, even though this decay scenario does not directly alter the baryon-to-photon ratio at BBN, CMB observations favor changes in the baryon energy density in the context of a Y decay, ultimately changing the predicted abundance of primordial elements. Furthermore, the presence of the hidden sector particle slightly increases the expansion rate during BBN and thereby alters the predicted primordial abundance of elements. Finally, scenarios in which the Y particle lifetime extends past the time of recombination have the potential to simultaneously increase the value of H_0 and decrease the cold dark matter energy density content that is preferred by CMB anisotropy data, ultimately decreasing the relative contribution of matter to the total present day energy density (Ω_m) inferred by the CMB.

The constraints derived in this work improve upon the limits derived in decaying cold dark matter (DCDM) models (e.g. [49–55]), where dark matter is composed of a stable component and a component that decays into DR. We improve upon the constraints derived in these studies with the inclusion of data from the third generation South Pole Telescope 2018 (SPT-3G) [56–58], Pantheon+ type Ia supernovae measurements [59], and bounds on the abundance of deuterium. More importantly, the parametrization that is commonly used in DCDM studies results in constraints that depend on the choice of prior for the particle lifetime when employing a Markov-chain Monte Carlo (MCMC) analysis. We choose to parametrize the amount of the decaying species with the quantity R_Γ, which is a measure of the Y particle energy density compared to all other species at the time when Γ_Y equals the expansion rate. With this parametrization, derived bounds on R_Γ are applicable to all short-lived decay scenarios and are not prior dependent. Therefore, the R_Γ parametrization employed in this work serves as a robust guide to how much DR can be injected prior to recombination.

Additionally, we derive adiabatic initial conditions for the DR perturbations in two common gauges: conformal Newtonian and synchronous gauge [60]. Since the DR is sourced by the decay of the Y particle, the DR energy density initially scales as a^{-1}, where a is the scale factor. Therefore, a naive application of adiabaticity would lead one to assume that $\delta_{\rm dr} = (1/4)\delta_\gamma$ in both conformal Newtonian and synchronous gauge, where $\delta_{\rm dr}$ and δ_γ are the fractional density perturbations in DR and photons, respectively. While this is indeed true in conformal Newtonian gauge, we find that $\delta_{\rm dr}$ is not initially equal to $(1/4)\delta_\gamma$ in synchronous gauge; there exists an attractor solution in synchronous gauge that sets $\delta_{\rm dr} = (17/20)\delta_\gamma$. This attractor solution quickly rectifies any incorrect initial condition and so other DCDM studies that neglected to set the correct initial condition for DR in synchronous gauge are still valid. Nevertheless, we include an in-depth discussion of these DR initial conditions and provide a generalized approach that demonstrates the presence of a nonintuitive attractor solution in synchronous gauge if there is energy transfer between two species.

This paper is organized as follows. In Sec. II we describe the model and parametrization of the decaying Y particle scenario, with Sec. II B containing a discussion of the subtleties of the initial conditions for DR perturbations. In Sec. III, we explore the primary effects that the decay has on the CMB temperature anisotropies and primordial abundances. We motivate the choice of likelihoods and priors for our MCMC analysis in Sec. IV, and Sec. V presents the results. A summary can be found in Sec. VI, and we include an Appendix that contains details of our model implementation in CLASS [61] (Appendix A), a determination of the initial condition for DR perturbations in synchronous gauge (Appendix B 1), as well as a derivation of generalized adiabatic initial conditions for two cases: non-interacting fluids (Appendix B 2) and fluids that exchange energy via a decay (Appendix B 3). The Appendix also includes calculations for $\Delta N_{\rm eff}$ resulting from the injection of DR (Appendix C).

II. DECAYING PARTICLE MODEL

A. Parametrization

The equations describing the evolution of the energy density of the Y particle (ρ_Y) and that of the injected dark radiation ($\rho_{\rm dr}$) are

$$\dot{\rho}_Y + 3H\rho_Y = -\Gamma_Y \rho_Y, \tag{1}$$

$$\dot{\rho}_{\rm dr} + 4H\rho_{\rm dr} = +\Gamma_Y \rho_Y, \tag{2}$$

where Γ_Y is the decay rate of the Y particle, $H \equiv \dot{a}/a$ with scale factor a, and an overdot denotes a proper time derivative.[1]

The physical quantities that we wish to constrain are the Y particle's decay rate and its maximum contribution to the energy density of the Universe. The maximum contribution of ρ_Y serves as a proxy for the amount of DR injected as well as a measure of the impact that the Y particle has on observables while acting as extra cold dark matter. We parametrize the maximum contribution that the Y particle makes to the energy density of the Universe with the quantity R_Γ defined as

$$R_\Gamma \equiv \frac{\rho_{Y,i}(a_i/a_\Gamma)^3}{\rho_{sr}(a_\Gamma) + \rho_m(a_\Gamma) + \rho_{\rm ncdm}(a_\Gamma)}, \tag{3}$$

where $\rho_{Y,i}$ is the initial energy density of the Y particle, ρ_m is the combined energy density of baryons and cold dark matter, ρ_{sr} is the combined energy density of photons and massless neutrinos, $\rho_{\rm ncdm}$ is the energy density of noncold dark matter (i.e. massive neutrinos), and the initial scale factor, a_i, is assumed to be deep in radiation domination. We assume that neutrinos are composed of two massless species and one massive species with $m_\nu = 0.06$ eV. R_Γ approximately describes the maximum ratio of ρ_Y to the total energy density, $\rho_Y/\rho_{\rm tot}$, if a_Γ is chosen such that $\Gamma_Y \simeq H(a_\Gamma)$. Therefore, we define a_Γ via the relation

$$\Gamma_Y = H_i \sqrt{\frac{\rho_{Y,i}\left(\frac{a_i}{a_\Gamma}\right)^3 + \rho_m(a_\Gamma) + \rho_{sr}(a_\Gamma) + \rho_{\rm ncdm}(a_\Gamma)}{\rho_{r,i}}}, \tag{4}$$

where $H_i \equiv H(a_i)$ and $\rho_{r,i} = \rho_{sr,i} + \rho_{{\rm ncdm},i}$ since massive neutrinos are initially relativistic. We note that Eq. (4) is not an exact statement of $\Gamma_Y = H(a_\Gamma)$ because ρ_Y does not evolve as a^{-3} up to a_Γ and we do not include contributions from $\rho_{\rm dr}$ in the computation of $H(a_\Gamma)$. However, for the level of ρ_Y contributions that we consider in this work, Eq. (4) provides a value for a_Γ such that $\Gamma_Y \approx H(a_\Gamma)$ without numerically solving for the evolution of ρ_Y.

We modify the public Boltzmann solver the Cosmic Linear Anisotropy Solving System (CLASS) [61] to solve Eqs. (1) and (2) when given initial values for ρ_Y and $\rho_{\rm dr}$. Determining the initial densities that generate decay scenarios with specified R_Γ and Γ_Y values could be accomplished with a shooting algorithm but, in the interest of simplicity, we choose to derive an analytic model that maps R_Γ and Γ_Y to initial conditions for ρ_Y and $\rho_{\rm dr}$. This analytic approach is described in Appendix A, and an example of the resulting evolution of ρ_Y and $\rho_{\rm dr}$ is provided in Fig. 1. Initially, ρ_Y mimics the evolution of standard nonrelativistic matter ($\rho_Y \propto a^{-3}$) until $a \approx a_\Gamma$ after which ρ_Y exponentially decreases. As the DR is being sourced by the Y particle decay, $\rho_{\rm dr} \propto a^{-1}$. However, soon after $a \approx a_\Gamma$, the Y particle decay no longer sources significant DR and thus $\rho_{\rm dr}$ evolves as standard radiation, $\rho_{\rm dr} \propto a^{-4}$. As we explore in the following section, the fact that $\rho_{\rm dr}$ evolves as a^{-1} even though the DR equation of state parameter is $1/3$ has interesting ramifications for the initial conditions of DR perturbations in synchronous gauge.

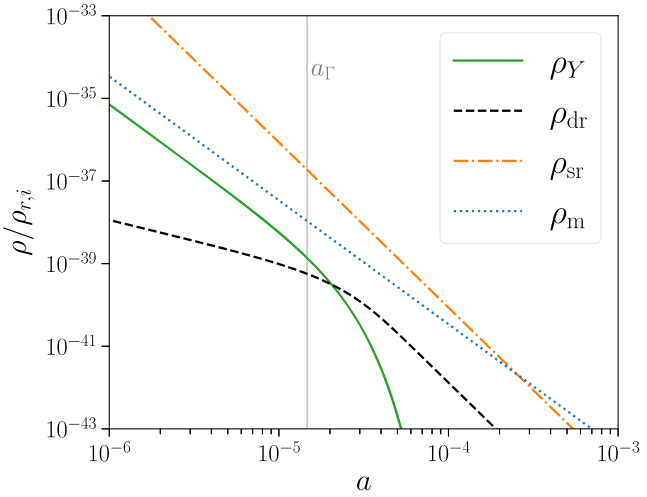

FIG. 1. Energy densities for a decay with $\Gamma_Y = 10^{6.5}$ Gyr^{-1} and $R_\Gamma = 0.01$. Here, ρ_Y is the energy density of the Y particle, $\rho_{\rm dr}$ is that of the DR, ρ_{sr} is the combined energy density of photons and massless neutrinos, and ρ_m is the combined energy density of baryons and cold dark matter. The Y particle energy density scales as $\rho_Y \propto a^{-3}$ until around $a \approx 10^{-5}$, at which point the decay rate overcomes the expansion rate. The DR energy density initially scales as $\rho_{\rm dr} \propto a^{-1}$ as it is sourced by the Y particle decay and then eventually transitions to scaling as a^{-4}. The vertical line marks a_Γ defined by Eq. (4).

B. Perturbations

The initial conditions that are implemented in CLASS for baryon, cold dark matter, photon, and neutrino perturbations are described in Ma and Bertschinger [60]. Here, we derive the superhorizon initial conditions during radiation domination for the scalar perturbations of the Y particle and the DR that is sourced by the decay of the Y particle. Since Boltzmann codes such as CLASS commonly evolve perturbations in synchronous gauge, we discuss the adiabatic initial conditions for the Y particle and DR in both conformal Newtonian gauge and synchronous gauge. The Friedmann-Lemaître-Robertson-Walker metric in conformal Newtonian gauge is

$$ds^2 = a(\tau)^2[-(1+2\Psi)d\tau^2 + \delta_{ij}(1-2\Phi)dx^i dx^j], \tag{5}$$

[1]Note that the right-hand sides of Eqs. (1) and (2) are proportional to $m_Y n_Y$, where m_Y and n_Y are the mass and number density of the Y particle, respectively. However, $m_Y n_Y = \rho_Y$ if the Y particle equation of state is $w_Y = 0$ [62].

where Φ and Ψ are scalar perturbations to the metric and τ is conformal time. The Friedmann-Lemaître-Robertson-Walker metric in synchronous gauge is

$$ds^2 = a^2(\tau)[-d\tau^2 + (\delta_{ij} + h_{ij})dx^i dx^j], \quad (6)$$

where the scalar part of the perturbation h_{ij} can be expressed in Fourier space as

$$h_{ij}(\vec{k},\tau) = \hat{k}_i\hat{k}_j h(\vec{k},\tau) + \left(\hat{k}_i\hat{k}_j - \frac{1}{3}\delta_{ij}\right)6\eta(\vec{k},\tau), \quad (7)$$

with $\vec{k} = k\hat{k}$ and k being the comoving wave number of a perturbation mode. Throughout this discussion, a superscript (s) or (n) denotes synchronous or conformal Newtonian gauge, respectively.

The DCDM module that is included in the public distribution of CLASS sets initial conditions for the fractional density perturbation of DCDM and DR in synchronous gauge as $\delta^{(s)}_{\rm dcdm} = (3/4)\delta^{(s)}_\gamma$ and $\delta^{(s)}_{\rm dr} = \delta^{(s)}_\gamma$, respectively, where $\delta^{(s)}_\gamma$ is the fractional density perturbation of photons. While this condition for $\delta^{(s)}_{\rm dcdm}$ is correct, there exists a different attractor solution for $\delta^{(s)}_{\rm dr}$ on superhorizon scales; the energy transfer to $\rho_{\rm dr}$ quickly pushes $\delta^{(s)}_{\rm dr}$ to $(17/20)\delta^{(s)}_\gamma$. This attractor promptly amends any incorrect initial condition for $\delta_{\rm dr}$ and therefore the incorrect default condition of $\delta^{(s)}_{\rm dr} = \delta^{(s)}_\gamma$ set by CLASS has no consequence (see the dotted lines in Fig. 2). For this work, we use $\delta^{(s)}_{\rm dr} = (17/20)\delta^{(s)}_\gamma$ as the initial condition in CLASS, and we enforce that perturbations are initialized at some initial scale factor, a_i, such that $\Gamma_Y/H(a_i) \leq 10^{-4}$. The factor of $\delta^{(s)}_{\rm dr}/\delta^{(s)}_\gamma = 17/20$ can be derived directly from the Boltzmann equations for DR in synchronous gauge (see Appendix B 1).

In both synchronous and conformal Newtonian gauge, adiabaticity is commonly assumed to mean that the quantity $\delta\rho_i/\dot{\bar{\rho}}_i$ is the same between all fluids, where $\bar{\rho}_i$ is the background energy density of a fluid and $\delta\rho_i = \rho_i - \bar{\rho}_i$. For noninteracting fluids, this implies $\delta_i/\delta_j = (1+w_i)/(1+w_j)$ on superhorizon scales. For example, this condition leads to the familiar relation $\delta_{\rm cdm} = (3/4)\delta_\gamma$ in both conformal Newtonian and synchronous gauges for noninteracting cold dark matter and photons.

Even for interacting fluids such as the DR sourced by the Y decay, adiabatic conditions are defined by $\delta\rho_i/\dot{\bar{\rho}}_i$ being the same between all fluids in conformal Newtonian gauge [63]. Since adiabatic initial conditions cannot source isocurvature initial conditions, the dynamics of these interacting fluids must preserve the equivalency of $\delta\rho_i/\dot{\bar{\rho}}_i$ between all fluids in conformal Newtonian gauge. However, because these fluids are interacting, $\dot{\bar{\rho}}_i/\overline{\rho_i} \neq -3H(1+w_i)$ and so the adiabatic condition does not result in the familiar relationship of $\delta_i/\delta_j = (1+w_i)/(1+w_j)$ on superhorizon scales. Solving Eq. (2) under the assumption of radiation domination and taking $\rho_Y \propto a^{-3}$, it follows that $\dot{\bar{\rho}}_{\rm dr}/\bar{\rho}_{\rm dr} = -1$ while the DR is being sourced, implying that $\delta^{(n)}_{\rm dr} = (1/4)\delta^{(n)}_\gamma$ initially even though DR and photons both have an equation of state parameter equal to 1/3. The solid dark line in Fig. 2 depicts this: while $\rho_{\rm dr} \propto a^{-1}$, the correct adiabatic condition for DR is $\delta^{(n)}_{\rm dr} = (1/4)\delta^{(n)}_\gamma$. Once the Y particle has sufficiently decayed away so that the DR is no longer being significantly sourced by the decay, $\rho_{\rm dr} \propto a^{-4}$ and adiabaticity leads to $\delta^{(n)}_{\rm dr} = \delta^{(n)}_\gamma$.

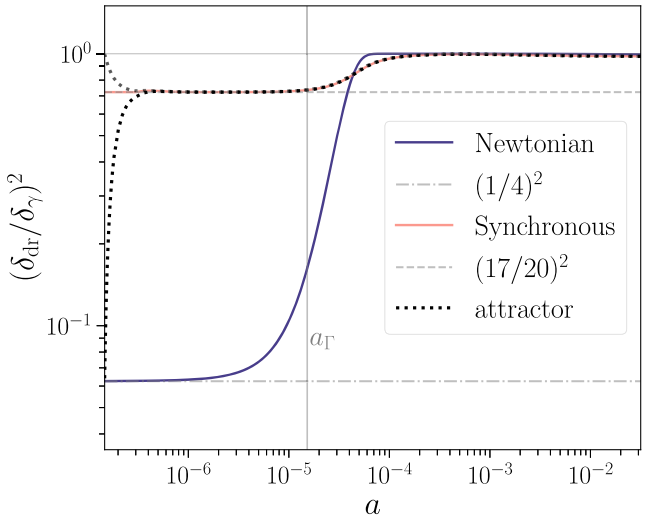

FIG. 2. Adiabatic initial conditions for a $k = 10^{-3}$ Mpc^{-1} perturbation mode and a decay with $\Gamma_Y = 10^{6.49}$ Gyr^{-1} and $R_\Gamma = 0.1$. In Newtonian gauge, adiabaticity requires that $\delta^{(n)}_{\rm dr} = (1/4)\delta^{(n)}_\gamma$ initially. However, in synchronous gauge there is an attractor solution of $\delta^{(s)}_{\rm dr} = (17/20)\delta^{(s)}_\gamma$. This attractor quickly fixes any incorrect initial condition for $\delta^{(s)}_{\rm dr}$ (dotted lines). In both gauges, $\delta_{\rm dr} = \delta_\gamma$ once the DR is no longer being sourced and $\rho_{\rm dr} \propto a^{-4}$.

When transforming from conformal Newtonian to synchronous gauge, most of the familiar adiabatic conditions are preserved [e.g. $\delta^{(s)}_Y = \delta^{(s)}_{\rm cdm} = (3/4)\delta^{(s)}_\gamma$]. However, this is not the case for DR: $\delta^{(n)}_{\rm dr}/\delta^{(n)}_\gamma \neq \delta^{(s)}_{\rm dr}/\delta^{(s)}_\gamma$. The underlying reason for this discrepancy is that the superhorizon limit means something different in synchronous gauge compared to conformal Newtonian gauge. Whereas $\delta^{(n)}$ approaches a constant nonzero value in the $k\tau \to 0$ limit, $\delta^{(s)}$ is proportional to $(k\tau)^2$ and vanishes in this limit [64].

To illustrate why this difference in superhorizon limits between gauges leads to $\delta^{(n)}_{\rm dr}/\delta^{(n)}_\gamma \neq \delta^{(s)}_{\rm dr}/\delta^{(s)}_\gamma$, we perform a

$k\tau$ expansion on the general gauge transformation between conformal Newtonian and synchronous gauge [60],

$$\delta_i^{(s)}(k) = \delta_i^{(n)}(k) - \alpha(k)\frac{\bar{\rho}_i'}{\bar{\rho}_i}. \tag{8}$$

Here, $\alpha(k) \equiv (h' + 6\eta')/2k^2$ and a prime denotes differentiation with respect to conformal time. We expand $\delta_i^{(n)}(k)$ in $k\tau$ such that it is composed of a zeroth order piece, $\delta_i^{(n),0}$, and a second order component, $C_i k^2\tau^2$. Similarly, $\alpha(k)$ is expanded such that $\alpha(k) \approx \alpha^0 + C_\alpha k^2\tau^2$. Equation (8) then becomes

$$\delta_i^{(s)}(k) \approx \left[\delta_i^{(n),0} + C_i k^2\tau^2\right] - [\alpha^0 + C_\alpha k^2\tau^2]\frac{\bar{\rho}_i'}{\bar{\rho}_i}. \tag{9}$$

Since adiabatic initial conditions in synchronous gauge have leading order terms proportional to $(k\tau)^2$, $\delta_i^{(n),0} = \alpha^0(\bar{\rho}_i'/\bar{\rho}_i)$.[2] It follows that

$$\delta_i^{(s)}(k) = C_i k^2\tau^2 - C_\alpha k^2\tau^2\frac{\bar{\rho}_i'}{\bar{\rho}_i} + \mathcal{O}(k^4\tau^4). \tag{10}$$

In other words, one cannot simply gauge transform the zeroth-order adiabatic solution in conformal Newtonian gauge in order to derive the correct adiabatic condition in synchronous gauge. The adiabatic solution in the superhorizon limit for synchronous gauge is the second order gauge transformation of the $(k\tau)^2$ terms in the adiabatic solution in conformal Newtonian gauge [63] (i.e. the transformation of C_i). Taking the ratio of Eq. (10) for two different species i and j, and assuming $\delta^{(n),0} = \alpha^0(\bar{\rho}'/\bar{\rho})$, we have

$$\frac{\delta_i^{(s)}}{\delta_j^{(s)}} = \frac{\delta_i^{(n),0}\left[\frac{C_i}{\delta_i^{(n),0}} - \frac{C_\alpha}{\alpha^0}\right]}{\delta_j^{(n),0}\left[\frac{C_j}{\delta_j^{(n),0}} - \frac{C_\alpha}{\alpha^0}\right]} + \mathcal{O}(k^4\tau^4). \tag{11}$$

Therefore, if the coefficient of the $(k\tau)^2$ term in the adiabatic initial condition for conformal Newtonian gauge is such that $C_i/C_j \neq \delta_i^{(n),0}/\delta_j^{(n),0}$, then the ratio of initial conditions for δ in synchronous gauge will not be equal to the same ratio in conformal Newtonian gauge.

In the case of noninteracting fluids, we show below in *case 1* that the usual adiabatic condition of $\delta_i/\delta_j = (1+w_i)/(1+w_j)$ is preserved even to second order in $k\tau$ in conformal Newtonian gauge, which means the same condition is true in synchronous gauge: $\delta_i^{(s)}/\delta_j^{(s)} = (1+w_i)/(1+w_j)$.

On the other hand, if there is some interaction between fluids such as energy exchange via a decay, we show in *case 2* that the initial condition for $\delta^{(n)}$ of the species that is being sourced has a $(k\tau)^2$ term such that $C_i/C_j \neq \delta_i^{(n),0}/\delta_j^{(n),0}$. Thus, the initial condition for this fluid in synchronous gauge does *not* result in the familiar adiabatic initial condition seen in Newtonian gauge: $\delta_i^{(s)}/\delta_j^{(s)} \neq (1+w_i)/(1+w_j)$. Similar results have been found for early dark energy models with a nonadiabatic sound speed [64].

1. Case 1 (no energy exchange)

Let us consider two fluids with energy densities ρ_1 and ρ_2. Additionally, there is a third fluid, ρ_d, which dominates the energy density of the Universe. If these three fluids are noninteracting, the evolution of their energy densities are entirely set by their respective equation of state parameters:

$$\dot{\rho}_d + 3H(1+w_d)\rho_d = 0, \tag{12}$$

$$\dot{\rho}_1 + 3H(1+w_1)\rho_1 = 0, \tag{13}$$

$$\dot{\rho}_2 + 3H(1+w_2)\rho_2 = 0. \tag{14}$$

Therefore, $H(a) \propto a^{-\frac{3}{2}(1+w_d)}$. In Appendix B 2 we solve the suite of Boltzmann equations in conformal Newtonian gauge for these three fluids using an iterative approach, and determine their respective adiabatic initial conditions to second order in $k\tau$. The resulting density perturbation for the jth fluid with equation of state parameter w_j is given by

$$\delta_j^{(n)} = 2\left(\frac{1+w_j}{1+w_d}\right)\Phi_p + \frac{2}{3}\left(\frac{1+w_j}{1+w_d}\right)\left[\frac{7+39w_d+63w_d^2+27w_d^3}{28+36w_d}\right](k\tau)^2\Phi_p, \tag{15}$$

where Φ_p is the initial value of the metric perturbation Φ. Equation (15) applies to all noninteracting fluids, including the dominant fluid. Here it can be seen that there is a zeroth-order term and a term of order $(k\tau)^2$, each having a coefficient proportional to $(1+w_j)/(1+w_d)$. The quantity in square brackets is solely dependant on w_d and therefore the same for fluids ρ_1, ρ_2, and ρ_d. The ratio of the zeroth-order component for any two species is $\delta_i^{(n),0}/\delta_j^{(n),0} = (1+w_i)/(1+w_j)$. Similarly, the ratio of the second order terms for two species is $C_i/C_j = (1+w_i)/(1+w_j)$. Therefore, according to Eq. (11), since $C_i/C_j = \delta_i^{(n),0}/\delta_j^{(n),0}$, the ratio of initial conditions in

[2]Note that this expression is another manifestation of adiabatic initial conditions in conformal Newtonian gauge: $\delta_i^{(n),0}/\delta_j^{(n),0} = (1+w_i)/(1+w_j)$.

synchronous gauge will equal that of the initial conditions in conformal Newtonian gauge. In other words, $\delta_i^{(s)}/\delta_j^{(s)} = (1+w_i)/(1+w_j) + \mathcal{O}(k^4\tau^4)$ for noninteracting fluids.

2. Case 2 (exchange via decay)

Next we will consider a similar scenario to that of *case 1*, except now we model species 1 as a massive species ($w_1 = 0$) decaying into species 2 with a decay rate Γ such that the energy densities of each fluid are set by

$$\dot{\rho}_d + 3H(1+w_d)\rho_d = 0, \tag{16}$$

$$\dot{\rho}_1 + 3H\rho_1 = -\Gamma\rho_1, \tag{17}$$

$$\dot{\rho}_2 + 3H(1+w_2)\rho_2 = +\Gamma\rho_1. \tag{18}$$

In a similar manner to case 1, we iteratively solve the perturbations equations for these fluids in Appendix B 3 to find the adiabatic initial conditions in conformal Newtonian gauge up to order $(k\tau)^2$. Since the dominant species is still noninteracting, the initial condition for $\delta_d^{(n)}$ is given by Eq. (15). Additionally, under the assumption that initial conditions are set sufficiently early, we take $\Gamma\rho_1 \ll H\rho_1$ initially. Under this assumption, Eq. (17) reduces to Eq. (13) for $w_1 = 0$ and therefore $\delta_1^{(n)}$ is described by Eq. (15) as well. Therefore, even though species 1 is decaying and exchanging energy with species 2, we find that $\delta_1^{(n)}/\delta_d^{(n)} = 1/(1+w_d)$ at second order[3] in $(k\tau)$.

In contrast, $\Gamma\rho_1$ is not initially negligible compared to $H\rho_2$ so the correct adiabatic initial condition for species 2 cannot be described by Eq. (15). Instead, the adiabatic initial condition for species 2 is

$$\delta_2^{(n)} = \left(\frac{1-w_d}{1+w_d}\right)\Phi_p + \mathcal{W}(k\tau)^2\Phi_p, \tag{19}$$

where $\mathcal{W}$ is a nontrivial constant that depends on w_d and w_2 [see Eq. (B45) in Appendix B 3]. Solving Eq. (18) analytically shows that $\rho_2(a) \propto a^{-\frac{3}{2}(1-w_d)}$. If we define an effective equation of state $w_{2,\mathrm{eff}} \equiv -(1/2)(w_d+1)$ for species 2, then $\rho_2 \propto a^{-3(1+w_{2,\mathrm{eff}})}$ and it can be seen in Eq. (19) that the zeroth-order term of $\delta_2^{(n)}$ is equal to $2\Phi_p(1+w_{2,\mathrm{eff}})/(1+w_d)$, as expected for adiabatic initial conditions. However, Eq. (19) demonstrates that $\delta_2^{(n)}/\delta_d^{(n)}$ is not equal to $(1+w_{2,\mathrm{eff}})/(1+w_d)$ at second order in $k\tau$. Therefore, comparing to any noninteracting fluid j, we find that $\delta_2^{(n),0}/\delta_j^{(n),0} = (1+w_{2,\mathrm{eff}})/(1+w_j)$, but $C_2/C_j \neq \delta_2^{(n),0}/\delta_j^{(n),0}$. According to Eq. (11), this means that the correct adiabatic initial condition for species 2 in synchronous gauge has $\delta_2^{(s)}/\delta_j^{(s)} \neq \delta_2^{(n)}/\delta_j^{(n)}$. This discussion demonstrates why we see $\delta_Y^{(n)}/\delta_\gamma^{(n)} = \delta_Y^{(s)}/\delta_\gamma^{(s)} = 3/4$ while $\delta_{\mathrm{dr}}^{(n)}/\delta_\gamma^{(n)} = 1/4$ but $\delta_{\mathrm{dr}}^{(s)}/\delta_\gamma^{(s)} = 17/20$.

[3]Note that this is equivalent to $\delta_1^{(n)}/\delta_d^{(n)} = (1+w_1)/(1+w_d)$ since $w_1 = 0$.

III. EFFECTS OF A Y DECAY

The decaying Y particle and the injected DR influence observables such as the CMB temperature anisotropy spectrum and the abundance of primordial elements. In this section, we describe the primary effects of a Y decay on such observables. Understanding these effects and how other cosmological parameters may be adjusted to mitigate them motivates our selection of observational datasets and will guide our interpretation of the MCMC results presented in Sec. V.

We discuss the effects of a Y decay for three different regimes: short lived, intermediate, and long lived. We refer to *short-lived* cases as those scenarios in which the characteristic scale factor, a_Γ, is larger than the scale factor at the end of BBN but much smaller than the scale factor of matter-radiation equality. For $R_\Gamma < 0.1$, this corresponds to Y particle lifetimes of $10^{-12.08}\ \mathrm{Gyr} \lesssim \tau_Y \lesssim 10^{-7}\ \mathrm{Gyr}$. *Intermediate* cases are defined as scenarios in which a_Γ is between the scale factor when the matter density is no longer negligible ($\rho_m/\rho_{\mathrm{tot}} \sim 0.05$) and that of recombination. These limits correspond to $10^{-7}\ \mathrm{Gyr} \lesssim \tau_Y \lesssim 10^{-3.22}\ \mathrm{Gyr}$. Finally, *long-lived* cases are those in which a_Γ is greater than the scale factor at recombination, which correspond to Y particle lifetimes of $\tau_Y \gtrsim 10^{-3.22}\ \mathrm{Gyr}$.

A. Short-lived regime

When the Y particles decay before recombination, the primary impact on the CMB arises from a change in the effective number of relativistic species, N_{eff}, due to the injected DR. In Appendix C, we determine this change to N_{eff} as a function of both R_Γ and Γ_Y, and find that ΔN_{eff} is purely a function of R_Γ for short-lived cases ($\Gamma_Y \gtrsim 10^7\ \mathrm{Gyr}^{-1}$) in which the injection of DR finishes deep in radiation domination (see Fig. 12 in Appendix C).

Therefore, bounds on ΔN_{eff} directly translate to limits on R_Γ for these short-lived cases. This enables one to derive an upper bound on R_Γ that is independent of any prior for Γ_Y within the short-lived regime. This is in contrast to DCDM models, which are usually described by the dark matter decay rate (Γ_{dcdm}) and the fraction of the total dark matter density that is unstable (f_{dcdm}). The ΔN_{eff} induced by DCDM is then determined by $\Delta N_{\mathrm{eff}} \propto \Gamma_{\mathrm{dcdm}}^{-1/2} f_{\mathrm{dcdm}}/(1-f_{\mathrm{dcdm}})$ [53]. Therefore, constraints on ΔN_{eff} translate to constraints on the combination of Γ_{dcdm} and f_{dcdm}; if f_{dcdm} increases while Γ_{dcdm} decreases, N_{eff} can be kept constant. Due to this degeneracy between f_{dcdm} and Γ_{dcdm}, derived bounds on f_{dcdm} are entirely dependent on the prior adopted for Γ_{dcdm}. Poulin *et al.* [51]

and Nygaard *et al.* [53] only consider $10^3\ \mathrm{Gyr}^{-1} < \Gamma_{\mathrm{dcdm}} < 10^6\ \mathrm{Gyr}^{-1}$ for short-lived cases, motivated by the fact that the inclusion of larger decay rates would lead to poor sampling convergence. Therefore, their reported bounds on f_{dcdm} cannot be applied to decay rates outside of this range. Moreover, Holm *et al.* [65] employ profile likelihoods to illustrate that the degeneracy between f_{dcdm} and Γ_{dcdm} in DCDM models introduces volume effects when employing an MCMC analysis, resulting in the unwanted smoothing out of features in posterior distributions. Not only that, but enforcing a prior on Γ_{dcdm} effectively places a nonphysical upper bound on f_{dcdm}, which prevents one from reporting accurate constraints on f_{dcdm} alone. The R_Γ parametrization used in this work bypasses these issues.

The injection of free-streaming DR increases N_{eff} and decreases the ratio of ρ_m to ρ_r at the time of recombination: $(\rho_m/\rho_r)_{\mathrm{rec}}$. The CMB temperature anisotropy spectrum is very sensitive to changes in $(\rho_m/\rho_r)_{\mathrm{rec}}$ via the early integrated Sachs-Wolfe (ISW) effect [66,67]. Therefore, an increase in $\omega_{\mathrm{cdm}} \equiv \Omega_{\mathrm{cdm}}h^2$ is necessary to keep $(\rho_m/\rho_r)_{\mathrm{rec}}$ unaltered, where $\Omega_{\mathrm{cdm}} \equiv \rho_{\mathrm{cdm},0}/\rho_{\mathrm{crit},0}$ and $h \equiv H_0/(100\ \mathrm{km\,s^{-1}\,Mpc^{-1}})$. Furthermore, the addition of DR increases the prerecombination expansion rate and thereby reduces the size of the sound horizon, r_s. The locations of the acoustic peaks in the CMB are set by the angular size of the sound horizon (θ_s), so a decrease in the angular diameter distance (d_A) is required to keep $\theta_s = r_s/d_A$ fixed. A decrease in d_A is partially accomplished by the enhancement in ω_{cdm} that was required to fix $(\rho_m/\rho_r)_{\mathrm{rec}}$, while any remaining change to d_A can be accomplished by increasing H_0.

Once ω_{cdm} and H_0 have been increased to keep $(\rho_m/\rho_r)_{\mathrm{rec}}$ and θ_s fixed, the remaining effects that a non-zero ΔN_{eff} has on the CMB are a change in the damping scale and a unique phase shift in the acoustic peaks [29–31,68]. Silk damping is affected because the photon diffusion length scales as $r_D \propto \sqrt{1/H}$, whereas the sound horizon scales as $r_s \propto 1/H$. Thus, enhancing H_0 to fix θ_s leads to an overall increase in the angular size of the diffusion length, θ_D, causing extra suppression on small angular scales of the CMB [30]. However, this suppression can be compensated for by amplifying the baryon content, ω_b, or the spectral tilt, n_s.[4] While employing Planck anisotropy data will effectively enforce that $(\rho_m/\rho_r)_{\mathrm{rec}}$ and θ_s remain fixed, the addition of SPT-3G data further aids in constraining changes in ω_b and n_s that are needed to accommodate the small-scale effects of a ΔN_{eff} induced by the Y decay. SPT-3G data are also sensitive to the extra phase shift caused by a nonzero ΔN_{eff} and can help constrain this effect.

In addition to influencing the CMB, Y decays in the short-lived regime have the potential to alter the abundance of primordial elements created during BBN. Even though we consider Y particle lifetimes that are sufficiently long such that $\Delta N_{\mathrm{eff}} = 0$ throughout BBN, the Y particle can contribute a non-negligible energy density to the Universe during BBN, which increases the expansion rate during BBN and alters when reactions freeze-out in a manner that cannot be modeled with a simple ΔN_{eff} [35]. The effect that the Y particle has on primordial abundances will be maximized for large R_Γ and short lifetimes. In order to ensure that N_{eff} is unaltered throughout BBN, we choose $\Gamma_Y = 10^{12.08}\ \mathrm{Gyr}^{-1}$ to be the largest decay rate that we consider. Additionally, we only consider values of $R_\Gamma \leq 0.1$ since any short-lived case with $R_\Gamma > 0.1$ corresponds to $N_{\mathrm{eff}} > 3.98$, which is ruled out by Planck temperature anisotropies alone. Therefore the ρ_Y contribution during BBN is maximized when $R_\Gamma = 0.1$ and $\Gamma_Y = 10^{12.08}\ \mathrm{Gyr}^{-1}$, for which the Y particle only makes up 0.9% of the total energy density at a temperature of $T = 0.01$ MeV. Thus, the Y particle has a small influence on primordial abundances. Nevertheless, we still account for this effect by altering the BBN code PArthENoPe-v3.0 [69] to include contributions from ρ_Y, and we provide CLASS with a table that was created using this modified version of PArthENoPe (details can be found in Sobotka *et al.* [35]). We also include direct measurements of the deuterium abundance in our analysis. In addition to constraining possible changes due to the presence of Y particles, these measurements also restrict changes in ω_b that are necessary to correct for excessive small-scale damping by the injected DR.

B. Intermediate regime

Changes to N_{eff} caused by injected DR are directly proportional to R_Γ for short-lived cases. However, once the decay rate falls below $\Gamma_Y \approx 10^7\ \mathrm{Gyr}^{-1}$, the ΔN_{eff} that results from a Y decay increases with decreasing Γ_Y for a fixed R_Γ (see Fig. 12 in Appendix C). This dependence on Γ_Y arises from how R_Γ is defined; R_Γ is a proxy for $\rho_{\mathrm{dr}}(a_\Gamma)/\rho_{\mathrm{tot}}(a_\Gamma)$ and, as matter becomes more significant, the same DR contribution relative to the total energy density implies a greater amount of DR relative to standard radiation. Therefore, for a given value of R_Γ, scenarios in the intermediate regime of $10^{3.22}\ \mathrm{Gyr}^{-1} \lesssim \Gamma_Y \lesssim 10^7\ \mathrm{Gyr}^{-1}$ require larger increases in ω_{cdm} compared to those of short-lived cases to fix $(\rho_m/\rho_r)_{\mathrm{rec}}$.

Furthermore, the impact of Y decays on CMB observations in the intermediate regime cannot be mimicked by increasing N_{eff} because perturbation modes that enter the horizon while the Y particles are still present affect the CMB on scales that are observable by *Planck*. Let us define the mode that enters the horizon when the decay rate surpasses the Hubble rate as $k_\Gamma \equiv a_\Gamma H(a_\Gamma)$. This mode

[4]Increasing ω_b also increases the helium abundance, which would further dampen anisotropies on small scales [30,35]. However, since the helium abundance is only logarithmically dependent on the baryon-to-photon ratio, increasing ω_b has the net effect of reducing small-scale damping.

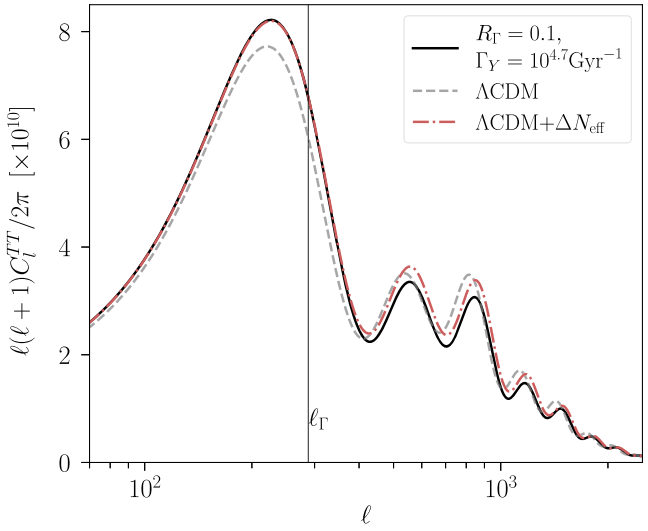

FIG. 3. Temperature anisotropy spectrum of an example Y decay in the intermediate regime (solid line). The vertical line, labeled ℓ_Γ, represents a scale that is dominated by the mode entering the horizon at a_Γ [i.e. $k_\Gamma = a_\Gamma H(a_\Gamma)$]. The dashed curve is the spectrum of a ΛCDM model and the dot-dashed curve is the spectrum of a ΛCDM model with $N_{\rm eff}$ matching the postdecay $N_{\rm eff}$ calculated using Eq. (C8). For scales with $\ell < \ell_\Gamma$, the decay spectrum is degenerate with that of ΛCDM + $N_{\rm eff}$.

contributes the most to temperature anisotropies at an angular scale of $\ell_\Gamma \approx k_\Gamma \chi_{\rm CMB}$, where $\chi_{\rm CMB}$ is the comoving distance to the surface of last scattering. For intermediate cases that have $\Gamma_Y \lesssim 10^{6.64}$ Gyr^{-1}, the corresponding angular scale ℓ_Γ falls in the observable range of the *Planck* satellite ($\ell_\Gamma \lesssim 2500$). Figure 3 depicts the temperature spectrum resulting from a Y decay with $\Gamma_Y = 10^{4.7}$ Gyr^{-1} and $R_\Gamma = 0.1$ (solid curve). Such a scenario has a mode of wave number $k_\Gamma \approx 0.021$ Mpc^{-1} entering the horizon at a_Γ, which dominates the power at an angular scale of $\ell_\Gamma \approx 288$ (vertical line). Large scales that enter the horizon after a_Γ (i.e. $\ell < \ell_\Gamma$) are primarily influenced by the decay via $\Delta N_{\rm eff}$ and so the decay spectrum is degenerate with a ΛCDM model with extra $N_{\rm eff}$ (dot-dashed line) for $\ell < \ell_\Gamma$. On the other hand, scales that enter the horizon before a_Γ are affected by the Y particle contributing to the dark matter content and so the decay spectrum is suppressed compared to ΛCDM for $\ell > \ell_\Gamma$. The Wess-Zumino Dark Radiation (WZDR) model, which generates similar scale-dependent modifications to the phase and amplitude of the acoustic peaks, can reduce the Hubble tension and is slightly favored by Planck and BAO data alone [70].

C. Long-lived regime

For decays in the long-lived regime, recombination occurs when no significant DR has been injected and the Y particle is behaving as stable nonrelativistic matter. Therefore, the Y particle *increases* $(\rho_m/\rho_r)_{\rm rec}$ and thus a reduction in $\omega_{\rm cdm}$ is needed to keep $(\rho_m/\rho_r)_{\rm rec}$ fixed.

While short-lived cases significantly alter the sound horizon via increases in $N_{\rm eff}$, the prerecombination contribution of $\rho_{\rm dr}$ to the expansion is insignificant for long-lived cases. Instead, the Y particle makes a non-negligible contribution to the prerecombination expansion and thereby reduces r_s. However, the reduction in $\omega_{\rm cdm}$ that is required to fix $(\rho_m/\rho_r)_{\rm rec}$ counters this effect and keeps r_s unchanged. The required reduction in $\omega_{\rm cdm}$ also amplifies the angular diameter distance to the CMB, d_A. Increasing H_0 can correct for this change to d_A and maintain the observed value of θ_s. The required adjustments to H_0 and $\omega_{\rm cdm}$ for decays in the long-lived regime both serve to decrease $\Omega_{\rm cdm} = \omega_{\rm cdm}/h^2$ and thereby decrease Ω_m. Therefore, compared to ΛCDM, decays with $\Gamma_Y \lesssim 10^{3.22}$ Gyr^{-1} result in a smaller value of $S_8 \equiv \sigma_8\sqrt{\Omega_m/0.3}$, where σ_8 is the root mean square of matter fluctuations on $8h^{-1}$ Mpc scales. This effect is how some studies have employed DCDM to address both the H_0 and S_8 tensions (e.g. [71]).

IV. ANALYSIS METHOD

We use a modified version of CLASS-v3.2[5] [61], coupled with MontePython-v3[6] [72,73] as our MCMC engine and employ a Metropolis-Hastings algorithm. We assume a flat prior on the base six cosmological parameters $\{\omega_b, \omega_{\rm cdm}, h, A_s, n_s, \tau_{\rm reio}\}$ and, unless otherwise specified, we use $R_\Gamma = [0.0, 0.1]$ and $\log_{10}(\Gamma_Y/\mathrm{Gyr}^{-1}) = [1.49, 12.08]$ for priors on decay parameters (see Table I). The chosen upper limit of $\log_{10}(\Gamma_Y/\mathrm{Gyr}^{-1}) < 12.08$ ensures that the decay occurs after BBN has finished such that $N_{\rm eff} = 3.044$ is constant throughout BBN. A lower limit of $\log_{10}(\Gamma_Y/\mathrm{Gyr}^{-1}) > 1.49$ ensures that Y particle lifetimes that extend past the time of recombination are considered. Smaller decay rates correspond to Y particle lifetimes that extend deep into matter domination such that the injected DR has no impact on observables. Such scenarios have been investigated elsewhere (e.g. [34,50,51]) and are not the primary focus of this work.

To constrain the effects that a Y decay has on the CMB temperature anisotropies, we employ *Planck* 2018 high-ℓTT, TE, EE, low-ℓTT, and low-ℓEE likelihood functions [1], as well as the third generation SPT-3G TT, TE, and EE data [56–58] adapted to the CLIK format.[7] To further constrain Ω_m, we employ the likelihood from BOSS DR12 [2] BAO analysis[8] as well as the

[5]https://github.com/alexsobotka/Class_YtoDR.
[6]https://github.com/brinckmann/montepython_public.
[7]https://github.com/SouthPoleTelescope/spt3g_y1_dist.
[8]While newer datasets are available, DR12 combined with CMB observations is the most effective at breaking the degeneracy between Ω_m and $r_d H_0$, where r_d is the sound horizon at the end of the baryonic-drag epoch [74].

TABLE I. Priors used in MCMC analyses.

$\log_{10}(\frac{\Gamma_Y}{\mathrm{Gyr}})$	[1.49, 12.08] (full) [3.14, 12.08] (prerecombination) [1.49, 3.24] (postrecombination)
R_Γ	[0, 0.1]
$10^{-2}\omega_b$	[2.0, 2.7]
ω_{cdm}	[0.1, 0.15]
h	[0.5, 0.85]
$\ln 10^{10} A_s$	[2.9397, 3.1497]
n_s	[0.933, 0.9953]
τ_{reio}	[0.01, 0.1103]

Pantheon + likelihood [75] based on uncalibrated type Ia supernovae [59].

As discussed in Sec. III A, the deuterium abundance provides additional constraints on ρ_Y during BBN and also serves as an independent constraint on ω_b. We include bounds on the primordial deuterium abundance from Cooke *et al.* [76]: $(\mathrm{D/H}) = (2.527 \pm 0.030) \times 10^{-5}$. However, this bound only includes measurement uncertainty. As in Sobotka *et al.* [35], we account for extra uncertainty in D/H from nuclear reaction rates by translating the bounds on the baryon-to-photon ratio reported by Cooke *et al.* [76], $\eta = (6.119 \pm 0.100) \times 10^{-10}$, to bounds on D/H. These limits on η include both measurement uncertainty and uncertainty associated with reaction rates. We translate these bounds to limits on the deuterium abundance by calculating D/H for a range of $5.8 \leq 10^{10}\eta \leq 6.88$ using PArthENoPe. Within this range, $\mathrm{D/H} \propto \eta^{-1.65}$. We use this fit to determine a new fractional uncertainty for D/H ($\sigma_{\mathrm{DH}}/\mathrm{DH} = 1.65 \times \sigma_\eta/\eta$), resulting in $(\mathrm{D/H}) = (2.527 \pm 0.068) \times 10^{-5}$. We utilize a Gaussian likelihood function for MontePython with a mean and standard deviation of $\mu_{\mathrm{DH}} = 2.527 \times 10^{-5}$ and $\sigma_{\mathrm{DH}} = 6.83 \times 10^{-7}$, respectively.

We consider MCMC chains with a Gelman-Rubin [77] criterion of $|R - 1| < 0.01$ as converged, and postprocessing of all chains was done using GetDist [78] by removing the first 30% of points as burn-in.

V. RESULTS

A. Full marginalized results

Figure 4 shows the posterior distributions for the decay parameters Γ_Y and R_Γ as well as ω_b, ω_{cdm}, H_0, and S_8 with 68% and 95% confidence level (CL) contours for various combinations of datasets. The posterior values for each parameter are reported in Table II. The vertical band in the 1D posterior for H_0 in Fig. 4 shows the 1σ and 2σ bounds reported by the SH_0ES collaboration ($H_0 = 73.30 \pm 1.04\ \mathrm{km\,s^{-1}\,Mpc^{-1}}$) [9], and the dashed line in the 1D posteriors represents a ΛCDM model constrained with only *Planck* 2018 high-ℓTT, TE, EE, low-ℓTT, and low-ℓEE data. The 1D posterior of $\log_{10}(\Gamma_Y/\mathrm{Gyr}^{-1})$ also contains hatched regions marking the different Y particle lifetime regimes introduced in Sec. III: short-lived (cross hatch), intermediate (diagonal hatch), and long-lived (circles).

The Γ_Y values depicted in Fig. 4 span a wide range of Y particle lifetimes from right after the end of BBN to about 30 million years after recombination. For this range of decay rates, Planck anisotropy data constrain $R_\Gamma < 0.0347$ (95% CL), which translates to $\rho_Y/\rho_{\mathrm{tot}} < 0.0204$ for the shortest lifetime we consider and $\rho_Y/\rho_{\mathrm{tot}} < 0.0291$ for the longest lifetime. The inclusion of SPT-3G data and bounds on the primordial deuterium abundance (Planck + SPT + D/H) tighten these bounds to $R_\Gamma < 0.0340$ (95% CL), which translates to $\rho_Y/\rho_{\mathrm{tot}} < 0.0200$ and $\rho_Y/\rho_{\mathrm{tot}} < 0.0286$ for the shortest and longest lifetimes, respectively. Figure 4 shows that Planck + SPT + D/H constraints are comparable to those of Planck in the short-lived regime. However, Planck + SPT + D/H enforces the tightest constraints on R_Γ for $\log_{10}(\Gamma_Y/\mathrm{Gyr}^{-1}) \approx 4$. These constraints relax once $\log_{10}(\Gamma_Y/\mathrm{Gyr}^{-1}) \lesssim 4$ because the effects of a Y decay in these scenarios can be compensated for with changes in ω_{cdm} and H_0. However, the inclusion of Pantheon+ and BAO data limit these changes in ω_{cdm} and H_0 and thus Planck + SPT + D/H + Pan + BAO bounds on R_Γ are stricter than those of Planck + SPT + D/H once $\log_{10}(\Gamma_Y/\mathrm{Gyr}^{-1}) \lesssim 2.5$. As a result, a larger fraction of samples that are favored by the data fall in the short-lived regime of $\log_{10}(\Gamma_Y/\mathrm{Gyr}^{-1}) \gtrsim 7$. Therefore, marginalizing over the entire range of Γ_Y yields $R_\Gamma < 0.0360$ (95% CL) for Planck + SPT + D/H + Pan + BAO, which is less constrained than the corresponding bound from Planck+ SPT + D/H. Being agnostic about Y particle lifetimes, this bound of $R_\Gamma < 0.0360$ (95% CL) translates to $\rho_Y/\rho_{\mathrm{tot}} < 0.0302$ over the full range of Γ_Y considered. However, as will be discussed in subsequent sections, constraints on R_Γ can be more stringent based on the specific regime under consideration.

As discussed in Sec. III, the addition of the Y particle decreases θ_s. While the manner by which the Y particle decreases θ_s depends on the Y particle lifetime, an increase in H_0 is always required to keep θ_s consistent with CMB data. For the full range of decay rates considered, Y decays constrained by Planck data alone give $H_0 = 68.03^{+0.73}_{-0.99}\ \mathrm{km\,s^{-1}\,Mpc^{-1}}$ (68% CL), whereas $H_0 = 67.29 \pm 0.61\ \mathrm{km\,s^{-1}\,Mpc^{-1}}$ (68% CL) for a ΛCDM model constrained by Planck. We find that the combination of Planck + SPT + D/H + Pan + BAO results in $H_0 = 68.24^{+0.52}_{-0.83}\ \mathrm{km\,s^{-1}\,Mpc^{-1}}$ (68% CL) for Y decays, only reducing the tension with SH_0ES from 5.2σ to 4.4σ.

Similarly, we find that Y decay scenarios marginalized over the full prior for Γ_Y does not help mitigate the S_8 tension. When considering the full combination of datasets (Planck + SPT + D/H + Pan + BAO), we find $S_8 = 0.828 \pm 0.012$ (68% CL) whereas $S_8 = 0.825^{+0.011}_{-0.012}$

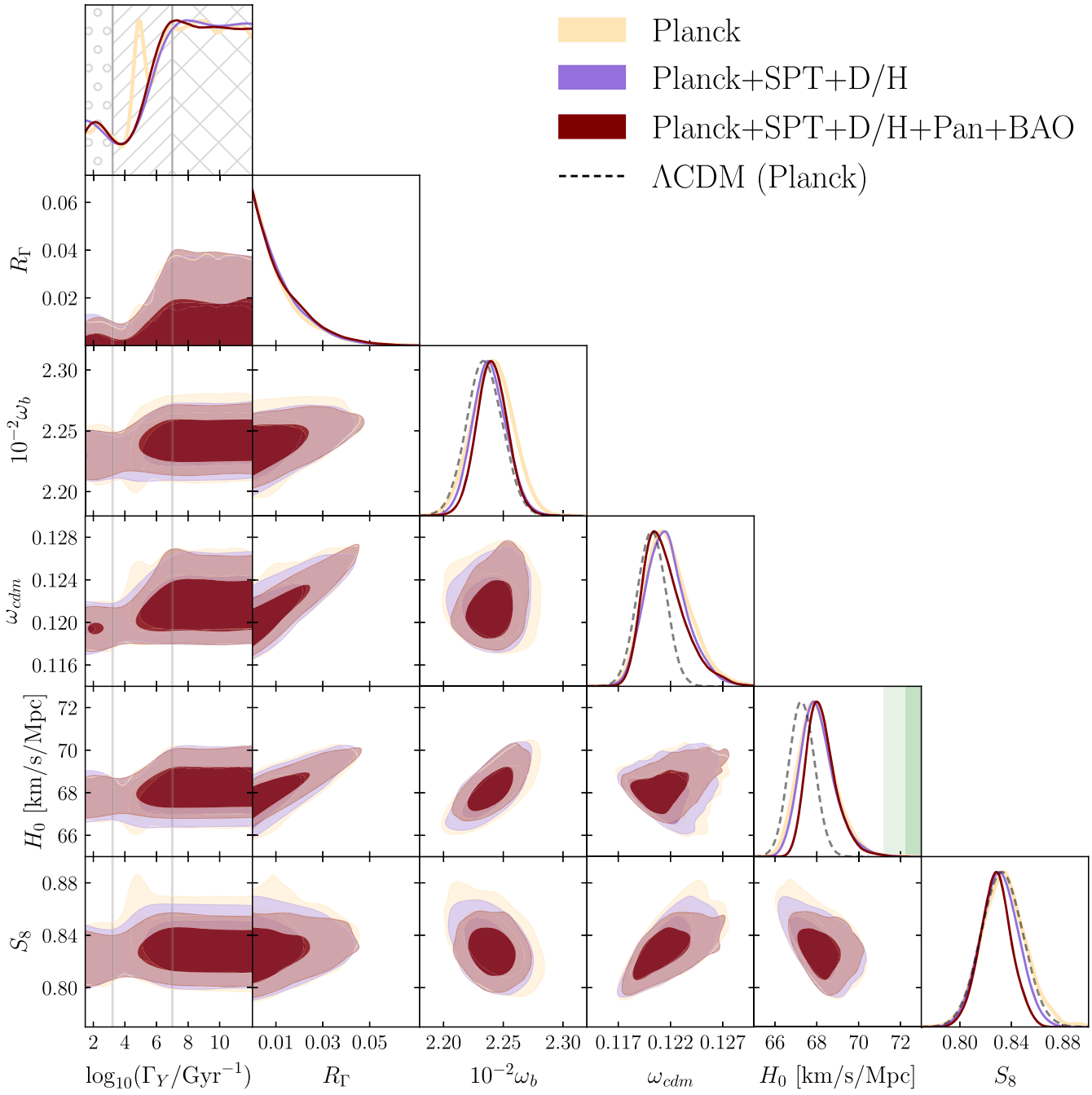

FIG. 4. 1D and 2D posterior distributions of decay and cosmological parameters for different combinations of *Planck* high-ℓTT, TE, EE, low-ℓTT, and low-ℓEE (Planck) data, SPT-3G 2018 TT, TE, and EE data (SPT), bounds on the observed deuterium abundance (D/H), Pantheon + data (Pan), and the BOSS DR12 likelihood (BAO). We include the 1D posteriors for ΛCDM constrained by Planck (dashed line). The vertical band shows the 1σ and 2σ bounds determined by SH_0ES ($H_0 = 73.30 \pm 1.04$ km s^{-1} Mpc^{-1}). Hatches in the 1D posterior for $\log_{10}(\Gamma_Y/\mathrm{Gyr}^{-1})$ mark the different Y particle lifetime regimes discussed in Sec. III: short-lived (cross hatch), intermediate (diagonal hatch), and long-lived (circles).

(68% CL) for a ΛCDM model constrained with Planck + SPT + D/H + Pan + BAO. Therefore, these decay scenarios do not lessen the tension between the value of S_8 inferred from the CMB and that of local measurements.

As discussed in Sec. III, the presence of the Y particle has different effects on observables depending how the Y particle lifetime compares to the times of matter-radiation equality or recombination. It is therefore more enlightening to analyze these results in the three regimes

TABLE II. Results for decay and cosmological parameters from MCMC analyses with a prior of $\log_{10}(\Gamma_Y/\mathrm{Gyr}^{-1}) = [1.49, 12.08]$, corresponding to those shown in Fig. 4. Uncertainties are reported at 68% CL and upper limits are given at 95% CL.

	ΛCDM (Planck)	Planck	Planck + SPT + D/H	Planck + SPT + D/H + Pan + BAO
R_Γ	⋯	< 0.0347	< 0.0340	< 0.0360
$\log_{10}(\Gamma_Y/\mathrm{Gyr}^{-1})$	⋯	⋯	⋯	⋯
H_0 [km s^{-1} Mpc^{-1}]	67.29 ± 0.61	$68.03^{+0.73}_{-0.99}$	$68.06^{+0.64}_{-0.94}$	$68.24^{+0.52}_{-0.83}$
S_8	0.833 ± 0.016	$0.834^{+0.016}_{-0.018}$	0.831 ± 0.015	0.828 ± 0.012
$10^{-2}\omega_b$	2.234 ± 0.015	2.241 ± 0.017	$2.239^{+0.013}_{-0.015}$	2.241 ± 0.013
ω_{cdm}	0.1202 ± 0.0014	$0.1218^{+0.0017}_{-0.0025}$	$0.1217^{+0.0016}_{-0.0022}$	$0.1214^{+0.0013}_{-0.0024}$
n_s	0.9644 ± 0.0044	$0.9684^{+0.0049}_{-0.0059}$	$0.9683^{+0.0045}_{-0.0058}$	$0.9693^{+0.0044}_{-0.0052}$

discussed in Sec. III: the short-lived ($\tau_Y \lesssim 10^{-7}$ Gyr), intermediate (10^{-7} Gyr $\lesssim \tau_Y \lesssim 10^{-3.22}$ Gyr) and long-lived ($\tau_Y \gtrsim 10^{-3.22}$ Gyr) regimes.

B. Short-lived regime

Figure 5 shows the posterior distributions for select parameters of an MCMC run with a prior of $\log_{10}(\Gamma_Y/\mathrm{Gyr}^{-1}) = [3.14, 12.08]$, corresponding to decay processes that finish before recombination and span the short-lived and intermediate regimes. For reference, a decay with $\Gamma_Y \approx 10^{3.22}$ Gyr^{-1} and $R_\Gamma < 0.1$ corresponds

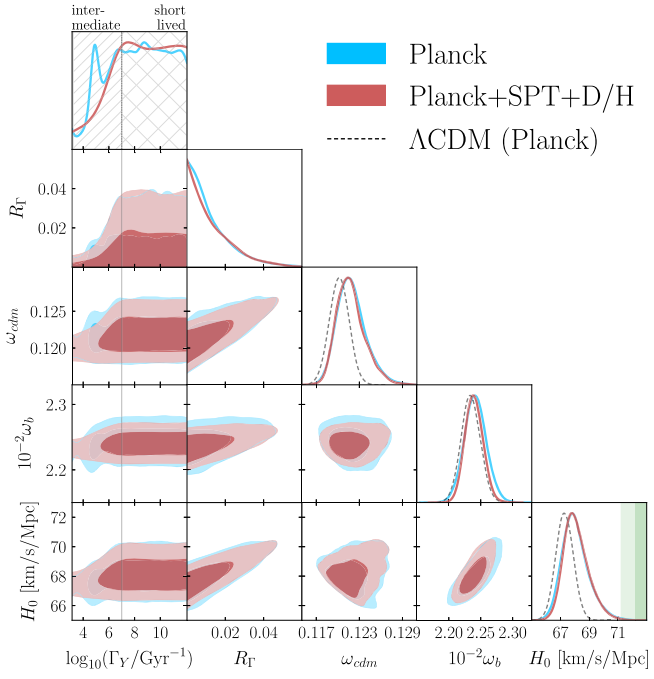

FIG. 5. 1D and 2D posterior distributions of decays in both the short-lived and intermediate regimes i.e. $\log_{10}(\Gamma_Y/\mathrm{Gyr}^{-1}) = [3.14, 12.08]$. The dashed line shows the 1D posteriors for ΛCDM constrained by Planck, and the vertical band shows the 1σ and 2σ bounds determined by SH_0ES ($H_0 = 73.30 \pm 1.04$ km s^{-1} Mpc^{-1}). Hatches in the 1D posterior for $\log_{10}(\Gamma_Y/\mathrm{Gyr}^{-1})$ mark the short-lived (cross hatch) and intermediate (diagonal hatch) regimes.

to a scenario with $a_\Gamma \approx a_{\mathrm{rec}}$. The lower bound of $\log_{10}(\Gamma_Y/\mathrm{Gyr}^{-1}) > 3.14$ ensures that we probe the transition from the intermediate regime to the long-lived regime. Values for select posteriors of this analysis are presented in Table III.

Figure 5 confirms the expectation for decays in the short-lived regime discussed in Sec. III A: Planck data exhibit a preference for larger values of H_0 and ω_{cdm} compared to those of a ΛCDM model (dashed line) to avoid altering θ_s and $(\rho_m/\rho_r)_{\mathrm{rec}}$. For the range of Γ_Y shown in Fig. 5, corresponding to decays that finish before recombination, the combination of Planck + SPT + D/H yields $\omega_{\mathrm{cdm}} = 0.1218^{+0.0014}_{-0.0023}$ (68% CL) and $H_0 = 68.10^{+0.67}_{-1.0}$ km s^{-1} Mpc^{-1} (68% CL) whereas a ΛCDM model constrained with Planck + SPT + D/H data lends $\omega_{\mathrm{cdm}} = 0.1200 \pm 0.0013$ (68% CL) and $H_0 = 67.33 \pm 0.54$ km s^{-1} Mpc^{-1} (68% CL).

Increasing ω_{cdm} to fix $(\rho_m/\rho_r)_{\mathrm{rec}}$ keeps the early ISW effect minimally altered. The observed Sachs Wolfe (SW) component of the temperature spectrum is the sum of the temperature monopole, Θ_0, and the gravitational perturbation, Ψ. As ω_{cdm} increases, Ψ becomes more negative, leading to a partial cancellation such that the sum of $\Theta_0 + \Psi$ is reduced. Therefore, increasing ω_{cdm} causes a suppression across all peaks. However, this effect can easily be reduced by increasing the amplitude, A_s. Indeed, for the

TABLE III. Posteriors for prerecombination decays (i.e. $\log_{10}(\Gamma_Y/\mathrm{Gyr}^{-1}) = [3.14, 12.08]$), corresponding to those shown in Fig. 5. Uncertainties are reported at 68% CL and upper limits are given at 95% CL.

	Planck	Planck + SPT + D/H
R_Γ	< 0.0357	< 0.0364
$\log_{10}(\frac{\Gamma_Y}{\mathrm{Gyr}})$	⋯	⋯
$H_0[\frac{\mathrm{km}}{\mathrm{s\cdot Mpc}}]$	$68.05^{+0.70}_{-1.1}$	$68.10^{+0.67}_{-1.0}$
ω_{cdm}	$0.1219^{+0.0015}_{-0.0023}$	$0.1218^{+0.0014}_{-0.0023}$
$\ln 10^{10} A_s$	3.051 ± 0.017	3.046 ± 0.016
$10^{-2}\omega_b$	2.242 ± 0.018	2.240 ± 0.014
n_s	0.9686 ± 0.0056	$0.9686^{+0.0046}_{-0.0059}$

range of $\log_{10}(\Gamma_Y/\mathrm{Gyr}^{-1}) = [3.14, 12.08]$, Planck data favor a slight increase in A_s: $\ln 10^{10} A_s = 3.051 \pm 0.017$ (68% CL) for Y decays, while $\ln 10^{10} A_s = 3.045 \pm 0.016$ (68% CL) for ΛCDM.

Once $(\rho_m/\rho_r)_{\mathrm{rec}}$ and θ_s have been fixed and A_s has been enhanced, there remains excessive Silk damping compared to the observed temperature spectrum. Therefore, as postulated in Sec. III A, the Planck data show a preference for a slightly larger value of ω_b in the short-lived regime compared to ΛCDM; increasing the baryon content will decrease the free streaming length of photons and mitigate any extra small-scale damping. However, altering ω_b also affects the height ratios of odd and even peaks in the temperature anisotropy spectrum. The inclusion of SPT data aid in constraining this effect on small scales. Additionally, the increase in ω_b favored by Planck data result in a change to the predicted abundance of primordial elements and so including bounds on the deuterium abundance also limits changes in ω_b. This can be seen in the ω_b vs $\log_{10}(\Gamma_Y/\mathrm{Gyr}^{-1})$ plane of Fig. 5.

Figure 5 demonstrates the benefit of the R_Γ parametrization used in this work compared to that commonly used in DCDM studies. As discussed in Sec. III A, the ΔN_{eff} arising from DCDM depends on the combination of Γ_{dcdm} and f_{dcdm}. Instead, ΔN_{eff} is exclusively dependent on R_Γ for short-lived decays and, as a result, there is a plateau in the R_Γ vs $\log_{10}(\Gamma_Y/\mathrm{Gyr}^{-1})$ plane of Fig. 5. The 2σ bound on this plateau is $R_\Gamma < 0.036$ which translates to a post-decay $N_{\mathrm{eff}} \leq 3.38$. This bound is more relaxed than the reported *Planck* 2018 TT, TE, EE + lowE bound of $N_{\mathrm{eff}} = 2.92^{+0.36}_{-0.37}$ (95% CL) [1]. However, the apparent discrepancy between these bounds stems from a difference in priors. The reported *Planck* 2018 bounds result from an analysis that allows for both positive and negative ΔN_{eff}, and Planck CMB observations exhibit a slight preference for negative ΔN_{eff}. The injected DR considered in this work only results in a positive ΔN_{eff}. For comparison, we perform an MCMC analysis applying Planck constraints to a ΛCDM model with a prior of $\Delta N_{\mathrm{eff}} = [0, 0.5]$. In doing so, we find that $N_{\mathrm{eff}} < 3.34$ (95% CL). This ΛCDM + ΔN_{eff} model increases N_{eff} during BBN, which results in a larger helium abundance. Simultaneous increases in both N_{eff} and the helium abundance conspire to produce excessive damping of small scale anisotropies and are therefore tightly constrained [35]. Therefore, the upper bound on N_{eff} for a ΛCDM model with only positive ΔN_{eff} is more stringent than that of Y decay scenarios in the short-lived regime.

A physically motivated extension to the Y decay model would be to consider additional DR that is not sourced by the decay of a Y particle. Such an ambient bath of DR would simply be modeled as a constant ΔN_{eff}. However, this would be a trivial extension to the short-lived regime given that constraints on short-lived cases are dominated by bounds on N_{eff}; the inclusion of a preexisting bath of DR would tighten the bounds on R_Γ that we have derived for the short-lived regime.

C. Intermediate regime

Figure 5 shows constraints on R_Γ becoming more stringent as the decay rate falls below $\log_{10}(\Gamma_Y/\mathrm{Gyr}^{-1}) \approx 7$. Similar to decays in the short-lived regime, Planck data mandate an increase in both H_0 and ω_{cdm} to effectively fix θ_s and $(\rho_m/\rho_r)_{\mathrm{rec}}$ for this intermediate regime of $\log_{10}(\Gamma_Y/\mathrm{Gyr}^{-1}) = [3.22, 7]$. However, in this intermediate regime, the ΔN_{eff} arising from a Y decay grows with decreasing Γ_Y for fixed R_Γ (see Fig. 12 in Appendix C). Consequently, the increase in ω_{cdm} required to fix $(\rho_m/\rho_r)_{\mathrm{rec}}$ grows as Γ_Y decreases. Therefore, for a given value of R_Γ, scenarios in the intermediate regime of $10^{3.22}\ \mathrm{Gyr}^{-1} \lesssim \Gamma_Y \lesssim 10^7\ \mathrm{Gyr}^{-1}$ require larger increases in ω_{cdm} compared to those of short-lived cases to fix $(\rho_m/\rho_r)_{\mathrm{rec}}$.

Fixing $(\rho_m/\rho_r)_{\mathrm{rec}}$ means the early ISW effect is minimally altered but, as discussed in Sec. V B, an increase in ω_{cdm} suppresses the SW component of the temperature spectrum by enhancing gravitational potential wells. For short-lived decays, this effect can be compensated for with a increase in the amplitude, A_s. However, in addition to this overall suppression, intermediate cases can simultaneously affect some CMB scales with ΔN_{eff} while other scales are suppressed by the presence of the Y particle (see Sec. III B). These effects work in tandem to foster asymmetry between the peak heights of the temperature spectrum.

To demonstrate this suppression and asymmetry, Fig. 6 shows the temperature spectra of three Y decays with $R_\Gamma = 0.02$ and various decay rates compared the spectrum of a ΛCDM model. Each spectrum assumes the same values for ω_b, A_s, n_s, and τ_{reio}, and we alter h and ω_{cdm} such that θ_s and $(\rho_m/\rho_r)_{\mathrm{rec}}$ are fixed. For the decay with $\Gamma_Y = 10^{5.5}\ \mathrm{Gyr}^{-1}$, ρ_Y is negligible by the time of recombination, and the only lasting effect is extra N_{eff} from the injected DR. Therefore, an increase in ω_{cdm} is required to fix $(\rho_m/\rho_r)_{\mathrm{rec}}$, and the early ISW component of the temperature spectrum (dotted line) is very similar to that of ΛCDM. However, increasing ω_{cdm} results in deeper gravitational potential wells and so the SW component (dot-dashed line) is suppressed compared to ΛCDM. Additionally, since ρ_Y is negligible by the times the modes that dominate the first and second peaks enter the horizon, there is no extra suppression from the Y particle and therefore the ratio of the first and second peak heights of the SW component is minimally altered.

As Γ_Y decreases within the intermediate regime, the required ω_{cdm} to fix $(\rho_m/\rho_r)_{\mathrm{rec}}$ increases. However, once Γ_Y falls below $10^4\ \mathrm{Gyr}^{-1}$, ρ_Y begins to contribute a non-negligible amount to $(\rho_m/\rho_r)_{\mathrm{rec}}$ and so less of an increase in ω_{cdm} is necessary. Therefore, for a fixed R_Γ, a decay with $\Gamma_Y \approx 10^4\ \mathrm{Gyr}^{-1}$ requires the maximum increase in ω_{cdm} and thereby results in the maximum suppression of the SW

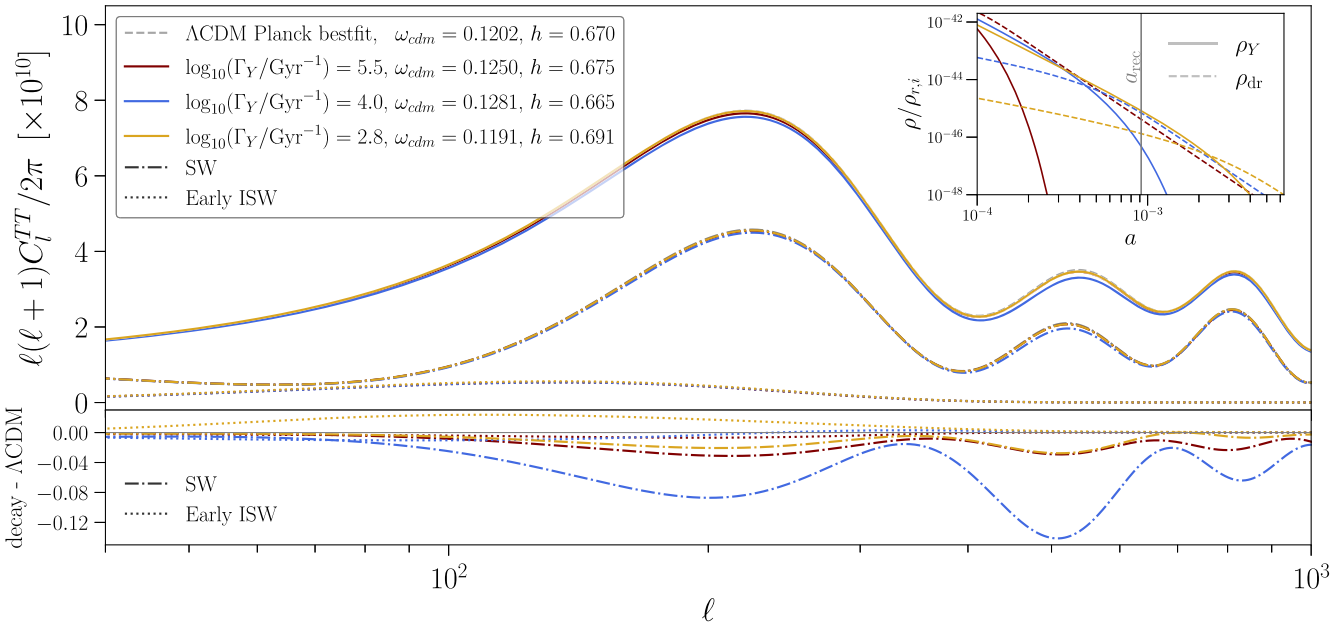

FIG. 6. Top panel: temperature anisotropy spectra of Y decay scenarios with $R_\Gamma = 0.02$ and different decay rates (solid curves) compared to that of a ΛCDM model (dashed curve). Unless otherwise specified, each spectrum is created with the TT, TE, EE, low-ℓEE best-fit values for the base six parameters reported by *Planck* 2018 [1]. For each decay scenario we increase h so that θ_s is fixed and we adjust ω_{cdm} to fix $(\rho_m/\rho_r)_{\mathrm{rec}}$. The dot-dashed and dotted curves depict the SW and early ISW components of each spectrum, respectively. Bottom panel: we plot the difference between the SW or early ISW component of each decay spectrum with that of the ΛCDM model. Top right: the evolution of energy densities ρ_Y (solid) and ρ_{dr} (dashed) for each decay scenario, with the vertical line marking the scale factor of recombination.

component of the temperature spectrum compared to other values of Γ_Y. This can be seen in the bottom panel of Fig. 6: fixing $(\rho_m/\rho_r)_{\mathrm{rec}}$ for a decay with $\Gamma_Y = 10^4$ Gyr^{-1} results in a significant suppression of the SW component.

Not only is there an overall suppression in the SW component for this decay with $\Gamma_Y = 10^4$ Gyr^{-1}, but also the second acoustic peak is further suppressed by the presence of the Y particle; as discussed in Sec. III B, if the mode that dominates the second peak enters the horizon while the Y particle is still present, the second acoustic peak will experience extra suppression. This ultimately results in a change in the height ratios between the first and second peak, thus making it more difficult to compensate for these changes with a simple shift in A_s. Instead, Fig. 5 shows that *Planck* data exhibit a preference for $R_\Gamma \to 0$ as $\log_{10}(\Gamma_Y/\mathrm{Gyr}^{-1}) \to 4$, ensuring both that suppression from the Y particle is negligible and that a minimal ΔN_{eff} is produced even for small values of Γ_Y.

When only applying *Planck* data, Figs. 4 and 5 show a peak in the posterior of Γ_Y around $\log_{10}(\Gamma_Y/\mathrm{Gyr}^{-1}) \approx 4.9$. Interestingly, a similar peak was observed in Poulin *et al.* [51]. Nygaard *et al.* [53] observed a slight plateau rather than a peak, and attributed this to their use of a stricter Gelman-Rubin convergence criterion for MCMC sampling compared to that of Poulin *et al.* [51]. However, by employing profile likelihoods, Holm *et al.* [65] pinpoint a best-fit value of $\log_{10}(\Gamma_Y/\mathrm{Gyr}^{-1}) = 4.763$ and explain the appearance of a plateau rather than a peak in the posteriors of Nygaard *et al.* [53] to volume effects from Bayesian methods. We find that, with the parametrization used in this work, there is indeed a preferential peak in the Γ_Y posterior even when enforcing the same convergence criteria as Nygaard *et al.* [53]. However, this preference for $\log_{10}(\Gamma_Y/\mathrm{Gyr}^{-1}) \approx 4.9$ is eliminated with the addition of SPT data and/or bounds on the primordial deuterium abundance.

To explain this preference for $\log_{10}(\Gamma_Y/\mathrm{Gyr}^{-1}) \approx 4.9$, we consider the resulting temperature anisotropy spectra of Y decay scenarios with three different decay rates. Figure 7 shows the temperature spectra for decays with $R_\Gamma = 0.03$ and $\log_{10}(\Gamma_Y/\mathrm{Gyr}^{-1})$ values of 5.64, 4.9, or 3.79. Included in the figure is an inset in the top right corner that depicts the Planck 1D posterior for $\log_{10}(\Gamma_Y/\mathrm{Gyr}^{-1})$ found in Fig. 4, where the solid vertical lines mark the decay rates of each decay scenario with corresponding colors. Figure 7 also includes the spectrum of a ΛCDM model (dashed line) with best-fit TT, TE, EE, low-ℓEE values for ω_b, ω_{cdm}, θ_s, A_s, n_s, and τ_{reio} reported by *Planck* 2018 [1]. Each decay scenario has the same best-fit values for ω_b, θ_s, n_s, and τ_{reio} as this ΛCDM model. Values for H_0 and ω_{cdm} have been adjusted for each decay scenario such that θ_s and $(\rho_m/\rho_r)_{\mathrm{rec}}$ are the same between all spectra. Additionally, the three decay spectra have been normalized to the second acoustic peak

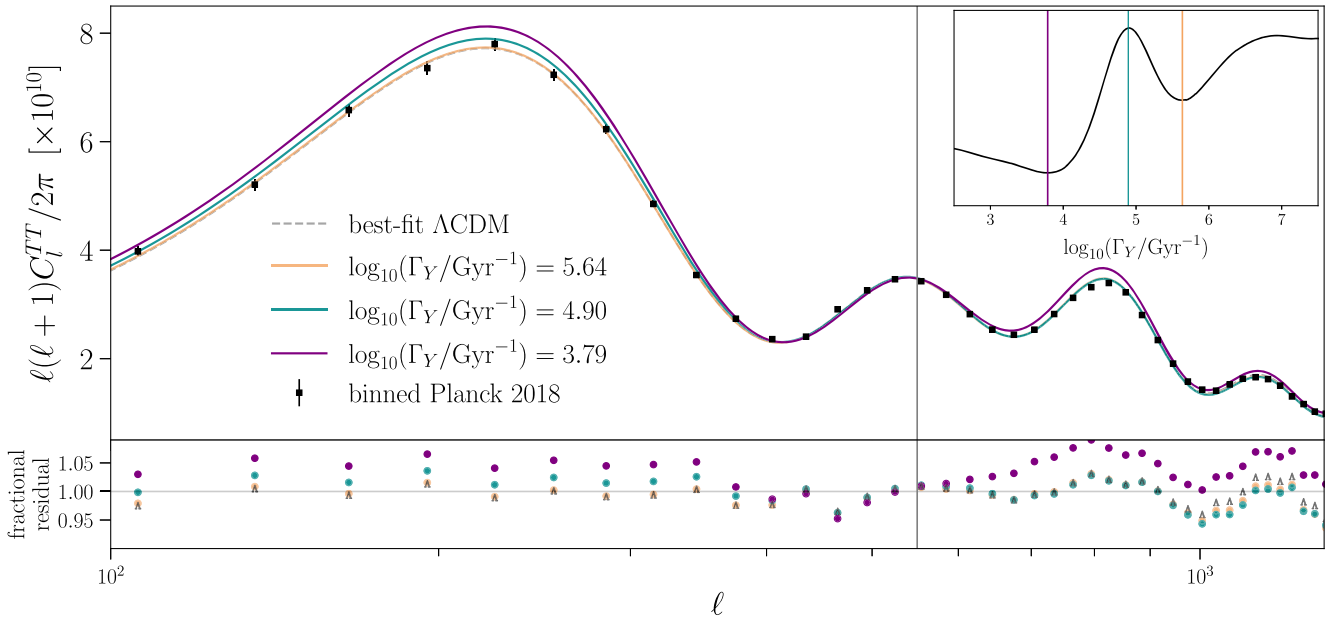

FIG. 7. Top panel: the dashed line shows the temperature anisotropy spectrum for a ΛCDM model with TT, TE, EE, low-ℓEE best-fit values for the base six parameters reported by *Planck* 2018 [1]. The three solid colored curves are the resulting spectra of Y decays with $R_\Gamma = 0.03$ and varying decay rates which are marked, respectively, as vertical lines in the top-right inset depicting the Planck 1D posterior of $\log_{10}(\Gamma_Y/\mathrm{Gyr}^{-1})$ from Fig. 4. Each spectrum has the same *Planck* 2018 best-fit values for ω_b, n_s, and τ_{reio}. For all spectra the values for H_0, ω_{cdm}, and A_s have been adjusted to keep θ_s, $(\rho_m/\rho_r)_{\mathrm{rec}}$, and the second peak height fixed, respectively. The *Planck* 2018 binned TT data are shown by the black squares with corresponding 1σ error bars. Bottom panel: fractional residuals of the best-fit ΛCDM (shown by "Λ" markers) and Y decay scenario (circles) with the binned *Planck* 2018 data. Of these scenarios, the decay with $\log_{10}(\Gamma_Y/\mathrm{Gyr}^{-1}) = 4.9$ is enhanced on large scales but suppressed on small scales compared to ΛCDM and therefore it is easier for the $\log_{10}(\Gamma_Y/\mathrm{Gyr}^{-1}) = 4.9$ decay to agree with Planck data by increasing n_s.

by augmenting A_s. Black points are the binned TT spectrum data provided by the Planck collaboration[9] and the lower panel of Fig. 7 depicts the fractional residuals between the ΛCDM spectrum (shown by the "Λ" markers) or decay spectra (colored circles) and these binned data.

Each decay scenario in Fig. 7 injects DR before recombination and thereby requires an increase in ω_{cdm} to fix $(\rho_m/\rho_r)_{\mathrm{rec}}$. Therefore, each decay spectrum in Fig. 7 experiences suppression across all peaks. Additionally, depending on the value of Γ_Y, the presence of the Y particle suppresses some scales more than others and leads to an asymmetry in peak heights between the first and second peak. By adjusting A_s to normalize the second peak height between all spectra, this asymmetry effect is apparent in Fig. 7. The $\log_{10}(\Gamma_Y/\mathrm{Gyr}^{-1}) = 5.64$ scenario requires the smallest increase in ω_{cdm} compared to the other decay rates shown in Fig. 7 and so the first peak is in good agreement with that of ΛCDM even after normalizing the second peak height. However, some small-scale suppression compared to ΛCDM is present for this $\log_{10}(\Gamma_Y/\mathrm{Gyr}^{-1}) = 5.64$ scenario due to the presence of the Y particle. On the other hand, the $\log_{10}(\Gamma_Y/\mathrm{Gyr}^{-1}) = 3.79$ decay spectrum necessitates the largest increase in ω_{cdm}, leading to a notable suppression across all acoustic peaks. The second acoustic peak is further suppressed because the mode that dominates this peak enters the horizon while the Y particle is still present. Therefore, the second acoustic peak is more suppressed compared to the first and third peaks and, by normalizing the second peak height with A_s, the first and third peaks of the $\log_{10}(\Gamma_Y/\mathrm{Gyr}^{-1}) = 3.79$ spectrum are enhanced compared to ΛCDM.

The decay rate of $\log_{10}(\Gamma_Y/\mathrm{Gyr}^{-1}) = 4.9$ is more compatible with the Planck data due to the resulting spectrum after changing H_0 and ω_{cdm} to fix θ_s and $(\rho_m/\rho_r)_{\mathrm{rec}}$, as well as adjusting A_s to normalize the second peak height. Compared to ΛCDM, the resultant spectrum of this particular decay rate exhibits enhancement on scales with $\ell \lesssim 546$, but a suppression on scales with $\ell \gtrsim 546$. The scale of $\ell_p \approx 546$ (vertical line in Fig. 7) is the ℓ value at which the temperature spectrum is invariant under changes in the spectral index, n_s. This indicates that increasing n_s is a straightforward method to align the resulting spectrum of a $\log_{10}(\Gamma_Y/\mathrm{Gyr}^{-1}) = 4.9$ decay with Planck data. Alternatively, a decrease in ω_b could also lead to agreement with Planck data; decreasing ω_b reduces the height separation between the first and second acoustic peaks.

[9] http://pla.esac.esa.int/pla/#cosmology.

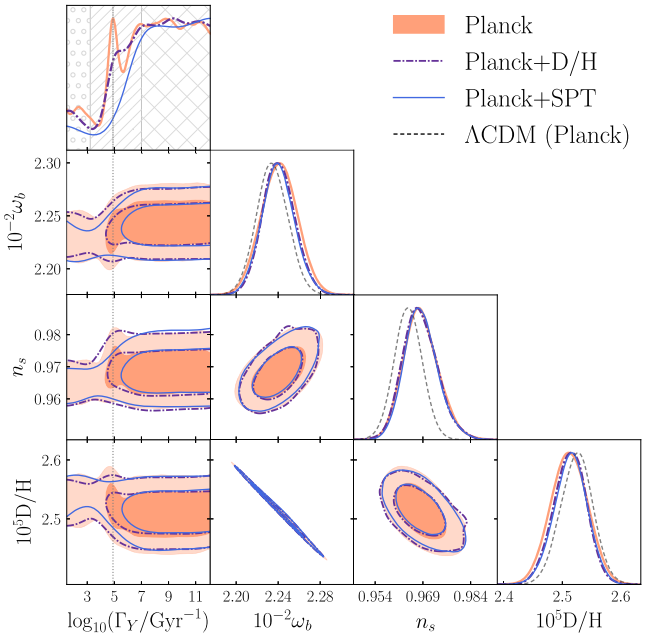

FIG. 8. 1D and 2D posterior distributions for Y decays with $\log_{10}(\Gamma_Y/\mathrm{Gyr}^{-1}) = [1.49, 12.08]$. Hatches in the 1D posterior for $\log_{10}(\Gamma_Y/\mathrm{Gyr}^{-1})$ mark the different Y particle lifetime regimes: short-lived (cross hatch), intermediate (diagonal hatch), and long-lived (circles). A decay rate of $\log_{10}(\Gamma_Y/\mathrm{Gyr}^{-1}) \approx 4.9$ agrees with Planck temperature anisotropies when accompanied with changes in ω_b and n_s. This preference is ruled out with the addition of SPT data and/or bounds on the abundance of primordial deuterium (D/H).

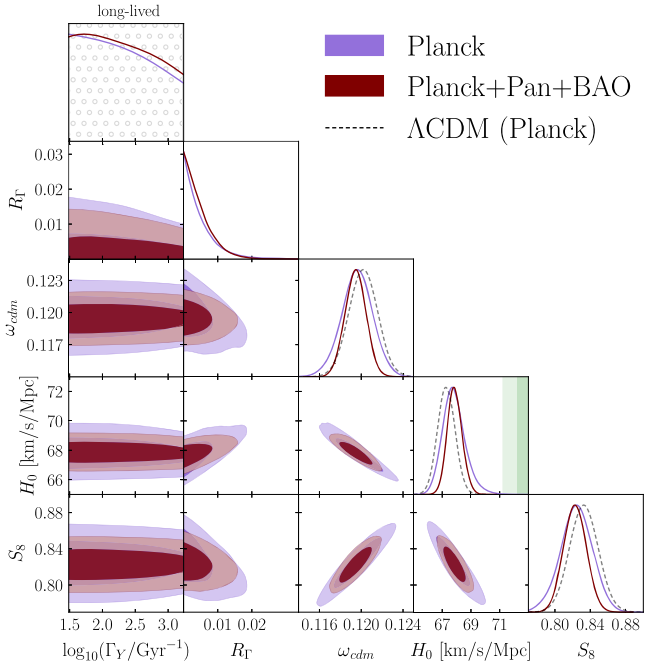

FIG. 9. 1D and 2D posterior distributions of late decays i.e. $\log_{10}(\Gamma_Y/\mathrm{Gyr}^{-1}) = [1.49, 3.24]$. The dashed line shows the 1D posteriors for ΛCDM constrained by Planck, and the vertical band shows the 1σ and 2σ bounds determined by SH_0ES ($H_0 = 73.30 \pm 1.04$ km s^{-1} Mpc^{-1}).

The preference for changes in ω_b and n_s to accommodate a $\log_{10}(\Gamma_Y/\mathrm{Gyr}^{-1}) \approx 4.9$ decay can be seen in Fig. 8, which depicts the 1D and 2D posterior distributions for MCMC analyses with $\log_{10}(\Gamma_Y/\mathrm{Gyr}^{-1}) = [1.49, 12.08]$ and $R_\Gamma = [0, 0.1]$. Figure 8 shows that Planck data permit larger R_Γ values for $\log_{10}(\Gamma_Y/\mathrm{Gyr}^{-1}) \approx 4.9$ when accompanied by a decrease in ω_b and an increase in n_s. However, this preference for $\log_{10}(\Gamma_Y/\mathrm{Gyr}^{-1}) \approx 4.9$ is lost with the inclusion of additional constraints from either SPT data or bounds on the abundance of deuterium. Changing ω_b alters the baryon-to-photon ratio and thereby the abundance of primordial deuterium, allowing for bounds on the deuterium abundance to constrain the changes in ω_b necessary to accommodate this special decay rate. Meanwhile, SPT data help constrain small-scale anisotropies of the temperature spectrum and therefore limits changes to both ω_b and n_s. In fact, SPT data are better at ruling out the preference for $\log_{10}(\Gamma_Y/\mathrm{Gyr}^{-1}) \approx 4.9$ since bounds on the deuterium abundance have no constraining power over n_s, as seen in the n_s vs $\log_{10}(\Gamma_Y/\mathrm{Gyr}^{-1})$ plane in Fig. 8.

D. Long-lived regime

To understand the effects of scenarios in which the Y particle lifetime extends past the time of recombination, we analyze the results of an MCMC run with $\log_{10}(\Gamma_Y/\mathrm{Gyr}^{-1}) = [1.49, 3.24]$, shown in Fig. 9. As discussed in Sec. III C, these long-lived scenarios require a reduction in ω_{cdm} to keep $(\rho_m/\rho_r)_{\mathrm{rec}}$ fixed and also require a larger value of H_0 to fix θ_s. Indeed, Fig. 9 demonstrates the preference that Planck data have for large H_0 and small ω_{cdm} compared to ΛCDM.

Figure 9 shows R_Γ becoming more constrained as $\log_{10}(\Gamma_Y/\mathrm{Gyr}^{-1}) \to 3$ (shorter lifetimes), corresponding to decay scenarios in which a_Γ approaches the scale factor of recombination. To understand why constraints tighten as $\log_{10}(\Gamma_Y/\mathrm{Gyr}^{-1}) \to 3$, we refer back to Fig. 6. Figure 6 depicts a long-lived scenario with $\Gamma_Y = 10^{2.8}$ Gyr^{-1} that requires a decrease in ω_{cdm} to fix $(\rho_m/\rho_r)_{\mathrm{rec}}$. Here it can be seen that, even though $(\rho_m/\rho_r)_{\mathrm{rec}}$ is fixed, the early ISW effect is still somewhat enhanced compared to ΛCDM (dotted lines). This enhancement is the result of the Y particle injecting DR after recombination, which results in the evolution of gravitational potentials. Additionally, the SW component of this long-lived spectrum is still suppressed compared to that of ΛCDM. For this particular decay rate of $\Gamma_Y = 10^{2.8}$ Gyr^{-1}, the energy density of the Y particle begins to deviate from a $\rho \propto a^{-3}$ scaling before recombination. Therefore, fixing $(\rho_m/\rho_r)_{\mathrm{rec}}$ does not result in a prerecombination expansion history equivalent to that of ΛCDM. Instead, fixing $(\rho_m/\rho_r)_{\mathrm{rec}}$ based on the value of ρ_Y at recombination leads to a total prerecombination dark

TABLE IV. Posteriors for post-recombination decays (i.e. $\log_{10}(\Gamma_Y/\mathrm{Gyr}^{-1}) = [1.49, 3.24]$), corresponding to those shown in Figs. 9 and 10. Uncertainties are reported at 68% CL and upper limits are given at 95% CL.

	Planck + Pan + BAO	Planck + Pan + BAO (ΔN_{eff})	Planck + Pan + BAO + SPT + D/H (ΔN_{eff})
R_Γ	< 0.0124	< 0.0115	< 0.0119
$H_0[\frac{\mathrm{km}}{\mathrm{s\cdot Mpc}}]$	$67.87^{+0.48}_{-0.54}$	$68.46^{+0.58}_{-0.78}$	$68.46^{+0.54}_{-0.74}$
ω_{cdm}	0.1195 ± 0.0010	$0.1212^{+0.0012}_{-0.0020}$	$0.1208^{+0.0012}_{-0.0017}$
S_8	0.823 ± 0.013	0.826 ± 0.013	0.825 ± 0.012
N_{eff}	...	< 3.32	< 3.29

matter content that is larger than that of ΛCDM. Thus, there is a suppression in the SW component of the $\Gamma_Y = 10^{2.8}\ \mathrm{Gyr}^{-1}$ curve in Fig. 6 compared to ΛCDM. As Γ_Y decreases, the value of ρ_Y at recombination will approach $\rho_{Y,i}(a_{\mathrm{rec}}/a_i)^3$ and so, after decreasing ω_{cdm} to fix $(\rho_m/\rho_r)_{\mathrm{rec}}$, the prerecombination expansion history will mimic that of ΛCDM. Therefore, Planck data exhibit a preference for larger R_Γ at smaller Γ_Y (longer lifetimes), as these scenarios are easily accommodated for with a simple decrease in ω_{cdm}.

Figure 9 confirms the expected effects of decays in the long-lived regime outlined in Sec. III C: the increase in H_0 and reduction in ω_{cdm} required by CMB observations for these long-lived cases result in a smaller value of Ω_m, and thereby S_8, compared to that of ΛCDM. *Planck* 2018 reported a TT, TE, EE + lowE bound of $S_8 = 0.834 \pm 0.016$ (68% CL) [1], whereas the long-lived posterior shown in Fig. 9 for Planck yields $S_8 = 0.824 \pm 0.018$ (68% CL). However, with the addition of data from Pantheon+ and BAO, long-lived cases are limited to $S_8 = 0.823 \pm 0.013$ (68% CL). Pantheon+ and BAO data constrain the reduction of Ω_m caused by decays in the long-lived regime as this reduction shifts the time of equality between matter and dark energy to earlier times. As a result, the long-lived regime is sufficiently restricted by Pantheon+ and BAO such that it does not reduce the tension between the CMB value of S_8 and that of local measurements. This result agrees with other studies that considered the effects of DCDM on S_8 (e.g. [34,71]).

Decay cases in the long-lived regime do not significantly increase the value of H_0 inferred from the CMB; we find Planck + Pantheon + BAO yields $H_0 = 67.87^{+0.48}_{-0.54}\ \mathrm{km\,s^{-1}\,Mpc^{-1}}$ (68% CL) for Y decays in the long-lived regime. Therefore, neither the short-lived nor long-lived regimes are successful in substantially mitigating the Hubble tension. Planck + Pan + BAO posterior values for the long-lived regime are presented in Table IV.

As mentioned in Sec. V B, DR need not be only sourced by the decay of a Y particle; it stands to reason that there could be an ambient background of DR that is not sourced by the Y decay. Such a DR background serves as an interesting extension to the long-lived cases considered here. Constraints on Y decays in the long-lived regime primarily derive from the necessary decrease in ω_{cdm} to fix $(\rho_m/\rho_r)_{\mathrm{rec}}$, but a DR background would increase ρ_r at recombination. Thus, a less significant decrease in ω_{cdm} would be necessary to fix $(\rho_m/\rho_r)_{\mathrm{rec}}$ while the Y particle is contributing to ρ_m at recombination, potentially relaxing the constraints enforced by Pantheon+ and BAO data.

To determine the extent to which constraints on long-lived cases relax in the context of an ambient DR background, we perform an MCMC analysis comparable to that shown in Fig. 9 but with the additional freedom of a variable and positive ΔN_{eff}. We assume priors of $R_\Gamma = [0, 0.1]$, $\log_{10}(\Gamma_Y/\mathrm{Gyr}^{-1}) = [1.49, 3.24]$, and $N_{ur} = [2.0328, 2.5328]$, where N_{ur} is the effective number of relativistic species excluding massive neutrinos and DR created by the decay of the Y particle. The contribution that the single massive neutrino species makes to N_{eff} is $N_{\mathrm{ncdm}} = 1.0132$, so this prior on N_{ur} corresponds to $\Delta N_{\mathrm{eff}} = [0, 0.5]$. This upper bound of $\Delta N_{\mathrm{eff}} < 0.5$ ensures that the we investigate the full extent of N_{eff} allowed by Planck data.

Figure 10 shows the 1D posterior distributions for ω_{cdm} and H_0 resulting from these analyses that include a DR background, and Table IV lists posterior values for select parameters. The dashed line shows the 1D posteriors of a ΛCDM model with fixed $\Delta N_{\mathrm{eff}} = 0$, while the dotted line shows those of a ΛCDM model with the prior of $\Delta N_{\mathrm{eff}} = [0, 0.5]$. In the absence of a DR background, the Planck data require a reduction in the parameter ω_{cdm} for long-lived scenarios due to the presence of the Y particle during recombination. With the incorporation of a DR background, Planck data favor an increase in ω_{cdm} because the additional DR component significantly contributes to the radiation energy density at the time of recombination. Comparing results from the ΛCDM + ΔN_{eff} model to those of a Y decay with variable ΔN_{eff}, the increase in ω_{cdm} required by Planck to fix $(\rho_m/\rho_r)_{\mathrm{rec}}$ is not as large for the decay as for the ΛCDM + ΔN_{eff} model. This is because the Y particle is still contributing to the matter density at recombination for long-lived cases and thus, for the same ΔN_{eff}, the increase in ω_{cdm} required by Planck to fix $(\rho_m/\rho_r)_{\mathrm{rec}}$ is not as large compared to that needed by a ΛCDM + ΔN_{eff} model. This can be seen in Fig. 10.

With the addition of a DR background, there is an overall reduction in the size of the sound horizon for these long-lived cases. Consequently, the Planck data favor an increase in H_0 to fix θ_s. The decrease in Ω_m required to match the

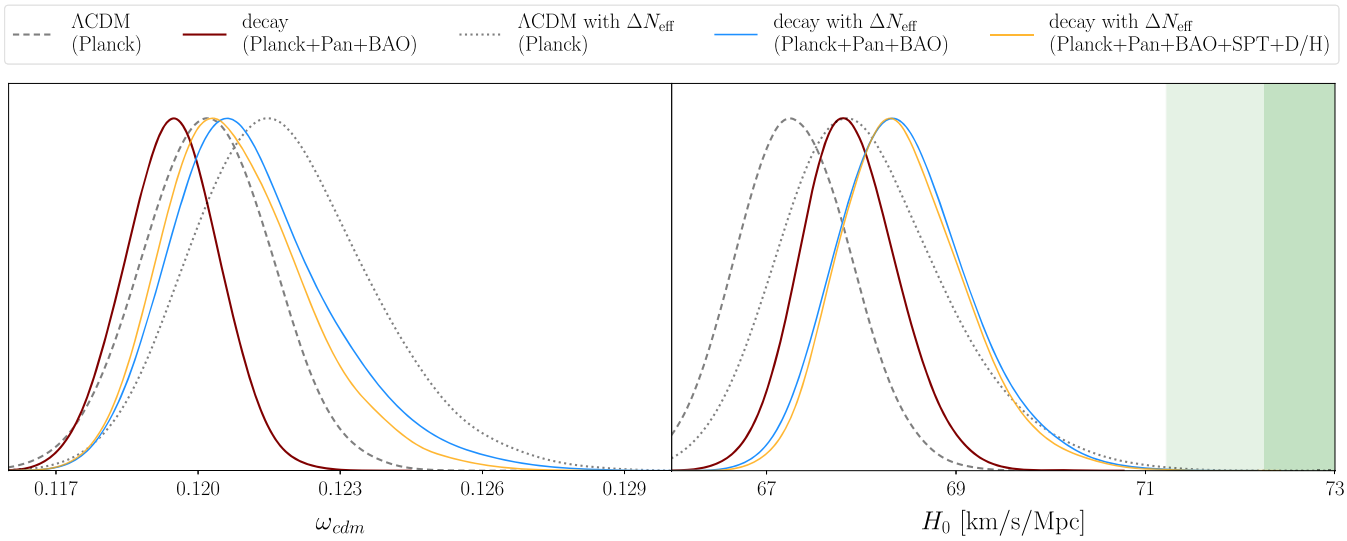

FIG. 10. Comparison between 1D posterior distributions resulting from decay scenarios in the long-lived regime (prior of $\log_{10}(\Gamma_Y/\mathrm{Gyr}^{-1}) = [1.49, 3.24]$). Dashed lines show resulting posteriors of a ΛCDM model with $\Delta N_{\rm eff} = 0$, while the dotted lines are those of a ΛCDM model with a variable $\Delta N_{\rm eff}$. The solid lines mark posteriors of either a decay model with only DR sourced by the decay (same as that shown in Fig. 9) or those of a model in which DR is sourced by the Y decay as well as an ambient DR background modeled by allowing $\Delta N_{\rm eff}$ to vary in the positive direction (prior of $\Delta N_{\rm eff} = [0, 0.5]$). The vertical band depicts the 1σ and 2σ bounds determined by SH_0ES ($H_0 = 73.30 \pm 1.04$ km s^{-1} Mpc^{-1}).

Planck data for long-lived Y particles without a DR background is constrained by Pantheon+ and BAO data. However, the inclusion of an ambient DR background results in an increase in both $\omega_{\rm cdm}$ and H_0, so Ω_m is minimally altered and thus the constraining power of Pantheon+ and BAO data on such scenarios is diminished. Therefore, the Planck + Pan + BAO posteriors shown in Fig. 10 for decays with a DR background are primarily the result of Planck constraints on $\Delta N_{\rm eff}$.

Naively one would expect the bounds on R_Γ to relax with the inclusion of a DR background since $(\rho_m/\rho_r)_{\rm rec}$ can be kept fixed even with significant contributions from ρ_Y at recombination. However, we find that limits on R_Γ become slightly more stringent with the inclusion of a DR background. For long-lived scenarios in which ρ_Y becomes negligible soon after recombination [i.e. $\log_{10}(\Gamma_Y/\mathrm{Gyr}^{-1}) \approx 3$], the Y decay injects new DR after recombination and enhances the early ISW effect. The addition of a DR background exacerbates these changes to the early ISW effect. Therefore, marginalizing over the full range of $\log_{10}(\Gamma_Y/\mathrm{Gyr}^{-1}) = [1.49, 3.24]$, we find that $R_\Gamma < 0.115$ (95% CL) for long-lived cases with a DR background constrained by Planck + Pan + BAO, whereas long-lived cases without a DR background yield $R_\Gamma < 0.124$ (95% CL) when constrained by Planck + Pan + BAO (see Table IV).

The inclusion of a DR background increases the expansion rate during BBN and thereby alters the predicted abundance of primordial elements. Therefore, including bounds on the primordial deuterium abundance should constrain this effect. However, for the level of $\Delta N_{\rm eff}$ that is allowed by Planck data, the predicted abundance of deuterium does not change significantly; ΛCDM constrained by Planck yields $10^5\mathrm{D/H} = 2.524 \pm 0.028$ (68% CL) whereas ΛCDM + $\Delta N_{\rm eff}$ constrained by Planck gives $10^5\mathrm{D/H} = 2.545 \pm 0.033$ (68% CL). Thus, the inclusion of bounds on the primordial deuterium abundance does not significantly constrain long-lived scenarios that contain a DR background. The inclusion of SPT + D/H data has a minimal impact on the constraints on $\Delta N_{\rm eff}$ and thereby the value of $\omega_{\rm cdm}$ needed to fix $(\rho_m/\rho_r)_{\rm rec}$, as can be seen in Fig. 10 and Table IV. Furthermore, the posterior for H_0 is not significantly altered with the addition of D/H limits. In Sec. III we note that the contribution of ρ_Y to Hubble during BBN can also affect primordial element abundances. However, for the long-lived regime, any contribution from ρ_Y during BBN is negligible so we neglect this effect on the deuterium abundance for long-lived scenarios that contain a DR background.

Coupled with the presence of an ambient DR background, Y particle decays in the long-lived regime only reduce the H_0 tension with SH_0ES to 4.15σ; we find that Planck + SPT + D/H + Pan + BAO yields $H_0 = 68.46^{+0.54}_{-0.74}$ km s^{-1} Mpc^{-1} (68% CL) for decays with a DR background in the long-lived regime.

VI. SUMMARY AND CONCLUSIONS

We obtain updated and comprehensive constraints on the injection of DR after the time of BBN by considering a massive hidden sector particle, called the Y particle, that decays into DR. We employ a modified version of the

Boltzmann solver CLASS-v3.2 [61] to model the effects of such a Y decay and, in doing so, we determine the existence of an attractor solution for DR perturbations in synchronous gauge. Under the common assumption that adiabatic initial conditions are set by equating $\delta\rho/\dot{\bar{\rho}}$ between all fluids, one would expect the fractional density perturbation of DR ($\delta_{\rm dr}$) to equal $1/4$ of the fractional density perturbation of photons (δ_γ) in both conformal Newtonian and synchronous gauge. However, in synchronous gauge, an attractor solution enforces $\delta_{\rm dr} = (17/20)\delta_\gamma$. We demonstrate that this attractor rectifies any incorrect initial condition set for $\delta_{\rm dr}$ and so all previous works remain valid (see Fig. 2). This attractor stems from the fact that initial conditions in conformal Newtonian gauge are dominated by zero-order terms in a $k\tau$ expansion, whereas the first nonvanishing term in the corresponding synchronous gauge initial conditions are of order $(k\tau)^2$. We derive initial conditions in conformal Newtonian gauge for species that interact via a decay and demonstrate that, for the fluid that is being sourced by the decay, the $(k\tau)^2$ term differs from that of other fluids such that the ratio of perturbations (δ_1/δ_2) is not preserved between gauges. If there is no energy exchange between fluids, then δ_1/δ_2 is preserved between gauges.

We determine constraints on the Y particle decay rate (Γ_Y) and the maximum contribution that the Y particle makes to the energy density of the Universe (R_Γ) by employing observations of CMB temperature and polarization anisotropies from both *Planck* 2018 [1] and SPT-3G [56–58], bounds on the primordial deuterium abundance [35,76], and data from Pantheon+ [59,75] and BAO observations from BOSS DR12 [2]. We consider Y particle lifetimes that range from right after the end of BBN to about 30 million years after recombination ($10^{-12.08}$ Gyr $< \tau_Y < 10^{-1.49}$ Gyr), ensuring that injection of DR occurs after BBN has completed.

In the short-lived regime of $\Gamma_Y \gtrsim 10^7$ Gyr^{-1} in which the Y particle decays during radiation domination, decays primarily affect the CMB via changes in $N_{\rm eff}$. For these short-lived cases, the $\Delta N_{\rm eff}$ that arises from injected DR is solely a function of R_Γ (see Fig. 12 in Appendix C). In comparison, the $\Delta N_{\rm eff}$ arising from DCDM models is determined by $\Delta N_{\rm eff} \propto \Gamma_{\rm dcdm}^{-1/2} f_{\rm dcdm}/(1 - f_{\rm dcdm})$ [53], where $\Gamma_{\rm dcdm}$ is the dark matter decay rate and $f_{\rm dcdm}$ is the fraction of total dark matter energy density that is unstable. Therefore, while $f_{\rm dcdm}$ can become unbounded by CMB observations as $\Gamma_{\rm dcdm}$ increases, the parametrization used in this work avoids these convergence issues; the same bound on R_Γ applies to all Γ_Y in the short-lived regime. We find a 2σ upper bound of $R_\Gamma < 0.036$ for $\Gamma_Y \gtrsim 10^7$ Gyr^{-1}, which translates to $\rho_Y/\rho_{\rm tot} < 0.0211$. These bounds are similar to those derived in Sobotka *et al.* [35] for the range of $10^{10.03}$ Gyr$^{-1} \lesssim \Gamma_Y \lesssim 10^{12.08}$ Gyr^{-1}, where it was found that $\rho_Y/\rho_{\rm tot} \leq 0.0235$ (95% CL) for a model in which the Y particle decays into a mixture of photons and DR.

As Γ_Y falls below 10^7 Gyr^{-1}, the $\Delta N_{\rm eff}$ that arises from a Y decay increases for fixed R_Γ and thus Planck data demand increasingly large enhancements to $\omega_{\rm cdm}$ in order to keep the early ISW effect relatively fixed. This increase in $\omega_{\rm cdm}$ results in more suppression of temperature anisotropies. Furthermore, Y decays in the intermediate regime can influence some CMB scales via $\Delta N_{\rm eff}$ while simultaneously suppressing other scales with the presence of the Y particle, thereby fostering increased asymmetry between peak heights in the temperature spectrum (see Sec. III B). Since it is difficult to compensate for these effects with changes in n_s or ω_b, CMB observations yield more stringent constraints on R_Γ in the intermediate regime of $10^{3.22}$ Gyr$^{-1} \lesssim \Gamma_Y \lesssim 10^7$ Gyr^{-1}. Even so, there is a special decay rate of $\Gamma_Y \approx 10^{4.9}$ Gyr^{-1} for which the increase in $\omega_{\rm cdm}$ required by Planck and the extra suppression from the Y particle alter the ratio of peak heights in such a way that can be compensated for by increasing n_s (see Sec. V C). This same preference for $\Gamma_Y \approx 10^{4.9}$ Gyr^{-1} was also observed in Poulin *et al.* [51] and Holm *et al.* [65]. However, the inclusion of SPT data restrict this necessary change in n_s and eliminates any preference for $\Gamma_Y \approx 10^{4.9}$ Gyr^{-1}.

For cases in which the Y particle decays before recombination ($10^{3.14}$ Gyr$^{-1} \lesssim \Gamma_Y \lesssim 10^{12.08}$ Gyr^{-1}), the injection of DR decreases the size of the sound horizon and so Planck data favor an increase in H_0 to fix θ_s. When only constraining with Planck, these prerecombination scenarios result in $R_\Gamma < 0.0357$ (95% CL). The addition of SPT data and bounds on the primordial deuterium abundance primarily limit changes in n_s or ω_b needed by intermediate cases, and thus marginalizing over the full prerecombination range of $10^{3.14}$ Gyr$^{-1} \lesssim \Gamma_Y \lesssim 10^{12.08}$ Gyr^{-1}, we find that Planck + SPT + D/H yields $R_\Gamma < 0.0364$ (95% CL). This bound on R_Γ translates to for $\rho_Y/\rho_{\rm tot} < 0.0305$. Consequently, these prerecombination decay scenarios are not successful at mitigating the Hubble tension; Planck + SPT + D/H results in $H_0 = 68.10^{+0.67}_{-1.0}$ km s^{-1} Mpc^{-1}, only bringing the tension between the CMB inferred value and results from SH_0ES from 5.2σ [1] to 4.4σ. Even with the inclusion of SPT data and bounds on the deuterium abundance, these limits on H_0 are in good agreement with those derived by Nygaard *et al.* [53] for short-lived cases.

Long-lived scenarios in which the Y particle lifetime extends past the time of recombination ($\Gamma_Y \gtrsim 10^{3.24}$ Gyr^{-1}) are required by Planck observations to be coupled with a decrease in $\omega_{\rm cdm}$ and an increase in H_0. The combination of these effects leads to an overall reduction in $\Omega_m = \omega_m/h^2$. Therefore, long-lived cases are subject to constraints from probes of Ω_m such as Pantheon+ [59,75] and BAO data from BOSS DR12 [2]. When applying Planck, Pantheon+, and BAO data, these long-lived scenarios are constrained such that $R_\Gamma < 0.0124$ (95% CL), corresponding to $\rho_Y/\rho_{\rm tot} < 0.011$ for $10^{1.49}$ Gyr$^{-1} \lesssim \Gamma_Y \lesssim 10^{3.24}$ Gyr^{-1}. In comparison, McCarthy and Hill [34] derived bounds on generic models

that convert some form of dark matter to DR after recombination by employing likelihoods for Planck, CMB lensing [79], BAO [2,80,81], Pantheon type Ia supernovae [82], and matter clustering from DES-Y3 [5]. McCarthy and Hill [34] parametrize the amount of dark matter that converts into DR with the parameter ζ and report a 2σ upper bound of $\zeta < 0.0748$. We translate[10] our Planck + Pan + BAO posteriors for Y decays in the long-lived regime to this parametrization and find a more stringent bound of $\zeta < 0.0321$ (95% CL). This discrepancy can be attributed to a difference in priors for the particle lifetime. Whereas the postrecombination prior of $10^{1.49}\ \mathrm{Gyr}^{-1} \lesssim \Gamma_Y \lesssim 10^{3.24}\ \mathrm{Gyr}^{-1}$ used here corresponds to $10^{-3.05} \lesssim a_\Gamma \lesssim 10^{-1.92}$, McCarthy and Hill [34] consider $10^{-4} < a_t < 10^4$ where $a_t \approx a_\Gamma$. McCarthy and Hill [34] see a peak in the posterior of a_t at $a_t \approx 1$ that broadens the marginalized posterior for ζ, leading to a bound on ζ that is much less stringent than that derived here.

We find that decays in the long-lived regime result in $S_8 = 0.823 \pm 0.013$ (68% CL) for Planck + Pan + BAO, only reducing the tension between DES-Y3 reported bounds and those inferred from the CMB from 2.5σ [1] to 2.3σ. Furthermore, compared to prerecombination decay cases, these long-lived scenarios are not as effective at mitigating the Hubble tension; Planck + Pan + BAO results in $H_0 = 67.87^{+0.48}_{-0.54}\ \mathrm{km\,s^{-1}\,Mpc^{-1}}$ (68% CL) for the long-lived regime, which agrees with results of comparable long-lived DCDM studies ([34,53]).

Since Pantheon+ BAO constraints on long-lived scenarios are driven by the need to decrease ω_{cdm} such that the early ISW effect is relatively fixed, introducing more radiation at recombination can relax these bounds. Including an ambient background of DR in addition to the DR sourced by the Y decay can enhance the resulting posterior for H_0 compared to long-lived cases that lack a DR background. We model a DR background by allowing a constant positive ΔN_{eff} and, with a prior of $\Delta N_{\mathrm{eff}} = [0, 0.5]$, we find that long-lived cases constrained by Planck + SPT + D/H + Pan + BAO yield $H_0 = 68.46^{+0.54}_{-0.74}\ \mathrm{km\,s^{-1}\,Mpc^{-1}}$ (68% CL). These long-lived scenarios with a DR background are more successful at mitigating the Hubble tension than prerecombination decay scenarios without a DR background.

Overall, Planck + SPT + D/H + Pan + BAO demonstrates less constraining power for Y decays in the short-lived regime, reflecting the fact that scenarios in which the Y particle lifetime is comparable to or greater than the time of recombination are strongly disfavored by CMB data and probes of Ω_m. Marginalizing over the full range of Y particle lifetimes considered in this work, Planck + SPT + D/H + Pan + BAO data yield $R_\Gamma < 0.0360$ (95% CL) which implies $\rho_Y/\rho_{\mathrm{tot}} < 0.0302$. Therefore, the Y particle is restricted to only contribute a maximum of about 3% of the energy density of the Universe. As a result, Y decay scenarios are sufficiently constrained such that they are not effective at mitigating the H_0 or S_8 tensions. Considering a DR background in addition to the DR sourced by Y decays in the long-lived regime can aid in bolstering H_0 further, but still fall far short at resolving the tension with measurements from SH_0ES [9].

This work affirms the notion that the production of relativistic particles of any kind after BBN is strongly constrained. The injection of photons and/or relativistic electrons has been thoroughly investigated ([36–42]) and these situations are subject to stringent constraints from measurements of primordial element abundances given their ability to photodisintegrate deuterium. Furthermore, the production of photons that do not photodisintegrate deuterium can introduce spectral distortions in the CMB and therefore the injection of new photons is restricted to be within the first $\sim 10^{-11}$ Gyr after the big bang [35]. Such photon injection reduces the ΔN_{eff} associated with DR injection and relaxes CMB constraints on the amount of DR present during recombination. However, to maintain consistency with the precisely measured present-day CMB temperature, such scenarios must alter the baryon-to-photon ratio during BBN and are therefore strongly constrained by measurements of the primordial deuterium abundance [35]. While the injection of DR alone is not significantly constrained by BBN, we find that the bounds placed on such scenarios by CMB anisotropy observations and probes of Ω_m are similar to the stringent bounds placed on scenarios that inject photons. In light of these results, it is evident that the production of any new free-streaming relativistic particles in the early Universe is highly constrained by cosmological observations. As a result, such extensions to ΛCDM cosmology are not capable of resolving the Hubble and S_8 tensions. This exemplifies the challenges faced when trying to resolve these tensions with early Universe modifications alone [83–85]. Even so, examples of models that succeed in addressing the H_0 and S_8 tensions with only prerecombination modifications to cosmic evolution do exist [70,86–90].

[10]We analytically relate R_Γ and Γ_Y to ζ by employing Eq. (A2) and taking $a_i = 10^{-14}$ and $\rho_Y(a_\Gamma) \approx \rho_{Y,i}(a_i/a_\Gamma)^3$. We evaluate $\rho_{r,i}$ assuming a CMB temperature of 2.7255 K and that three neutrino species are initially relativistic. $\rho_{m,i}$ is determined using our posterior distribution for ω_m. It follows that ζ is determined by Eq. (9) of McCarthy and Hill [34] by setting their model parameters of κ and a_t equal to 2 and a_Γ, respectively, and determining $\rho_{\mathrm{cdm},0}$ from our posterior distribution for ω_{cdm}. This transformation is applied to our MCMC chains to obtain a marginalized distribution for ζ.

ACKNOWLEDGMENTS

This work utilized the Longleaf Computing Cluster owned by the University of North Carolina at Chapel Hill. A. C. S. and A. L. E. received support from NSF Grants No. PHY-1752752 and No. PHY-2310719 during this investigation. T. L. S. is supported by NSF Grants No. 2009377 and No. 2308173 and thanks the Center for

Cosmology and Particle Physics (NYU) where part of this work was completed.

APPENDIX A: MODEL IMPLEMENTATION

We modify CLASS to solve Eqs. (1) and (2) when given initial values for ρ_Y and $\rho_{\rm dr}$. To determine these values, we derive a mapping from R_Γ and Γ_Y to $\rho_{Y,i}$ and $\rho_{{\rm dr},i}$. Combining Eqs. (3) and (4) determines a_Γ/a_i as a function of Γ_Y and R_Γ, which can then be inserted back into Eq. (3) to solve for $\rho_{Y,i}$. However, the function for a_Γ/a_i must be determined separately for the regimes in which the massive neutrinos are relativistic or nonrelativistic at a_Γ. The evolution of $\rho_{\rm ncdm}$ can be approximated by a broken power law that pivots from scaling as a^{-4} to a^{-3} at some pivot scale factor a_p:

$$\rho_{\rm ncdm}(a) = \begin{cases} \rho_{{\rm ncdm},i}\left(\frac{a_i}{a}\right)^4 & \text{if } a < a_p \\ \rho_{{\rm ncdm},i}\left(\frac{a_i}{a_p}\right)^4\left(\frac{a_p}{a}\right)^3 & \text{if } a > a_p \end{cases}. \tag{A1}$$

Here, $a_p = a_0(T_0/T_p)(4/11)^{1/3}$ and $T_p = m_\nu/3.15$ [91], with m_ν being the mass of the massive neutrino species. We take the minimal assumption that neutrinos are composed of two massless species and one massive species with $m_\nu = 0.06$ eV. Combining Eqs. (A1) and (3), we find that

$$\frac{\rho_{Y,i}}{\rho_{r,i}} = R_\Gamma \times \begin{cases} \left(\frac{a_i}{a_\Gamma} + \frac{\rho_{m,i}}{\rho_{r,i}}\right), & a_\Gamma < a_p \\ \left[\epsilon\left(\frac{a_i}{a_\Gamma}\right) + \frac{\rho_{m,i}}{\rho_{r,i}} + (1-\epsilon)\left(\frac{a_i}{a_p}\right)\right], & a_\Gamma > a_p, \end{cases} \tag{A2}$$

where $\epsilon \equiv \rho_{sr,i}/\rho_{r,i}$ and $\rho_{r,i} = \rho_{sr,i} + \rho_{{\rm ncdm},i}$. Inserting this initial condition back into Eq. (4), we obtain the quartic equation

$$\left(\frac{a_\Gamma}{a_i}\right)^4 + c\left(\frac{a_\Gamma}{a_i}\right) + d = 0, \tag{A3}$$

where

$$d = -\left(\frac{H_i}{\Gamma_Y}\right)^2(R_\Gamma + 1), \tag{A4}$$

$$c = d \times \begin{cases} \left(\frac{\rho_{m,i}}{\rho_{r,i}}\right) & \text{if } a_\Gamma < a_p \\ \left[\frac{\rho_{m,i}}{\rho_{r,i}} + (1-\epsilon)\left(\frac{a_i}{a_p}\right)\right] & \text{if } a_\Gamma > a_p \end{cases}. \tag{A5}$$

Equation (A3) can be solved analytically. Therefore, under the assumption of a_i being deep in radiation domination such that H_i is completely determined by $\rho_{r,i}$, a value for a_Γ/a_i can be determined when equipped with values for R_Γ, Γ_Y, $\rho_{m,i}$, and $\rho_{r,i}$. From there, $\rho_{Y,i}$ is determined via Eq. (A2). Finally, solving Eq. (2) under the assumption of radiation domination such that $H(a) \approx H_i(a/a_i)^{-2}$ leads to $\rho_{{\rm dr},i} = (\Gamma_Y/3H_i)\rho_{Y,i}$. We modify CLASS to derive these initial conditions for ρ_Y and $\rho_{\rm dr}$ when given values for R_Γ and Γ_Y. Note that Eq. (A1) is only used when relating R_Γ and Γ_Y to initial conditions; we do not modify the default calculations for $\rho_{\rm ncdm}$ in CLASS.

APPENDIX B: INITIAL CONDITIONS

1. Initial conditions for DR perturbations

We can derive the attractor initial condition for $\delta_{\rm dr}^{(s)}$, where the superscript (s) denotes synchronous gauge, by analytically solving the Boltzmann equations. The scalar perturbation equations for the Y particle and DR follow from the continuity and Euler equations and, in synchronous gauge, these result in

$$\delta_{\rm dr}^{\prime(s)} = -\frac{4}{3}\theta_{\rm dr}^{(s)} - \frac{4}{3}\left(\frac{h'}{2}\right) + a\Gamma_Y\frac{\rho_Y}{\rho_{\rm dr}}(\delta_Y^{(s)} - \delta_{\rm dr}^{(s)}), \tag{B1}$$

$$\theta_{\rm dr}^{\prime(s)} = \frac{k^2}{4}\delta_{\rm dr}^{(s)} - a\Gamma_Y\frac{3\rho_Y}{4\rho_{\rm dr}}\left(\frac{4}{3}\theta_{\rm dr}^{(s)} - \theta_Y^{(s)}\right). \tag{B2}$$

Here, a prime denotes a derivative with respect to conformal time and we have assumed that anisotropic stress is initially negligible. Assuming initial conditions are set during radiation domination, $\delta_\gamma^{(s)} = -(2/3)C(k\tau)^2$ and $h = C(k\tau)^2$ [60], where C is an arbitrary constant. As demonstrated in Sec. II B, if the evolution of an interacting fluid's energy density is unaffected by its interaction, then δ_i/δ_γ is the same in both synchronous and conformal Newtonian gauge, where δ_i is the density perturbation of the interacting fluid. Since $\rho_Y \propto a^{-3}$ initially, we know $\delta_Y^{(s)} = (3/4)\delta_\gamma^{(s)}$ and $\theta_Y^{(s)} = 0$. Additionally, if we take $H(a) = H_i(a/a_i)^{-2}$, then the initial evolution of $\rho_{\rm dr}$ can be determined by solving Eq. (2) analytically: $\rho_{\rm dr}(a) = (\Gamma_Y\rho_{Y,i}/3H_i)(a/a_i)^{-1}$. It follows that

$$\Gamma_Y\frac{\rho_Y}{\rho_{\rm dr}} = 3H. \tag{B3}$$

For adiabatic initial conditions, the DR perturbations will take the same form as standard radiation in that the first nonvanishing terms in a power series expansion in $(k\tau)$ for $\delta_{\rm dr}^{(s)}$ and $\theta_{\rm dr}^{(s)}$ are

$$\delta_{\rm dr}^{(s)} = D(k\tau)^2, \qquad \theta_{\rm dr}^{(s)} = Ek^4\tau^3, \tag{B4}$$

where D and E are constants. Recalling that $h = C(k\tau)^2$, $\delta_Y^{(s)} = (3/4)\delta_\gamma^{(s)} = -(1/2)C(k\tau)^2$, $\theta_Y^{(s)} = 0$, and that $\rho_Y/\rho_{\rm dr}$ is given by Eq. (B3), it follows that Eqs. (B1) and (B2) reduce to the algebraic equations of

$$2Dk^2\tau = -\frac{4}{3}Ek^4\tau^3 - \frac{2}{3}(2Ck^2\tau) - 3k^2\tau\left(\frac{C}{2} + D\right), \tag{B5}$$

$$3Ek^4\tau^2 = \frac{1}{4}Dk^4\tau^2 - 3Ek^4\tau^2. \tag{B6}$$

Solving Eqs. (B5) and (B6), we find that

$$D = 24E, \tag{B7}$$

$$E = -\frac{17C}{8(90 + k^2\tau^2)} \approx -\frac{17C}{720}. \tag{B8}$$

Therefore, $\delta_{\rm dr}^{(s)} = -(17/30)C(k\tau)^2$ and $\delta_{\rm dr}^{(s)}/\delta_\gamma^{(s)} = (17/20)$. We enforce this initial condition in the perturbation module of CLASS. Note that while this derivation does not formally prove $\delta_{\rm dr}^{(s)}/\delta_\gamma^{(s)} = (17/20)$ is an attractor solution, the numerical solution shown in Fig. 2 confirms that $\delta_{\rm dr}^{(s)}$ quickly converges to $(17/20)\delta_\gamma^{(s)}$.

2. Generalized initial conditions for noninteracting species

We employ an iterative approach to derive a general expression for adiabatic initial conditions of scalar perturbations in conformal Newtonian gauge. We consider three noninteracting species with energy densities ρ_1, ρ_2, and ρ_d, where ρ_d is assumed to dominate the energy density of the Universe. Since these fluids do not exchange energy, the evolution of their energy densities are determined by their respective equation of state parameters w_1, w_2, and w_d [see Eqs. (12)–(14)].

The perturbation equations for these species can be derived by perturbing the covariant form of Eqs. (12)–(14). We treat each species as a perfect fluid with an energy momentum tensor of

$${}^{(i)}T^{\mu\nu} = p_i g^{\mu\nu} + (\rho_i + p_i)u^\mu_{(i)}u^\nu_{(i)}, \tag{B9}$$

where i denotes each individual fluid, p_i is the pressure of the fluid, and $u^\mu_{(i)} \equiv dx^\mu/d\lambda$ is the fluid's four velocity. Since these fluids are noninteracting

$$\nabla_\mu({}^{(i)}T^\mu_\nu) = 0. \tag{B10}$$

The perturbation equations are found by evaluating Eq. (B10) with the perturbed conformal Newtonian metric in Eq. (5) and introducing perturbations to the energy density of each fluid $\rho_i(t,\vec{x}) = \rho_i^0(t)[1 + \delta_i(t,\vec{x})]$, where $\rho_i^0(t)$ is the background energy density of each fluid and $\delta_i(t,\vec{x}) \equiv \delta\rho_i/\rho_i^0$ is the fractional density perturbation of a fluid. We also introduce perturbations to the four-velocity of each fluid: $u^0 = (1-\Psi)$ and $u^j_{(i)} = (1-\Psi)V^j_{(i)}$, where $V^j_{(i)} \equiv dx^j/dt$ is the peculiar velocity of fluid i.

The $\nu = 0$ component of Eq. (B10) reduces to

$$\frac{{\rm d}\delta_i}{{\rm d}t} + (1+w_i)\frac{\theta_i}{a} + 3(1+w_i)\frac{{\rm d}\Phi}{{\rm d}t} = 0, \tag{B11}$$

where $\theta_i \equiv a\partial_j V^j_{(i)}$ is the divergence of the fluid's conformal velocity. The divergence of the spatial component ($\nu = j$) of Eq. (B10) results in

$$\frac{{\rm d}\theta_i}{{\rm d}t} + (1-3w_i)H\theta_i + \frac{\nabla^2\Psi}{a} + \frac{w_i}{1+w_i}\frac{\nabla^2\delta_i}{a} = 0. \tag{B12}$$

We apply Eqs. (B11) and (B12) to the three noninteracting fluids we are considering and the resulting suite of equations that we solve is

$$a^2E(a)\delta_1'(a) + (1+w_1)\tilde{\theta}_1(a) + 3(1+w_1)a^2E(a)\Phi'(a) = 0, \tag{B13}$$

$$a^2E(a)\tilde{\theta}_1'(a) + (1-3w_1)aE(a)\tilde{\theta}_1(a) + \tilde{k}^2\Phi(a) - \left(\frac{w_1}{1+w_1}\right)\tilde{k}^2\delta_1(a) = 0, \tag{B14}$$

$$a^2E(a)\delta_2'(a) + (1+w_2)\tilde{\theta}_2(a) + 3(1+w_2)a^2E(a)\Phi'(a) = 0, \tag{B15}$$

$$a^2E(a)\tilde{\theta}_2'(a) + (1-3w_2)aE(a)\tilde{\theta}_2(a) + \tilde{k}^2\Phi(a) - \left(\frac{w_2}{1+w_2}\right)\tilde{k}^2\delta_2(a) = 0, \tag{B16}$$

$$a^2E(a)\delta_d'(a) + (1+w_d)\tilde{\theta}_d(a) + 3(1+w_d)a^2E(a)\Phi'(a) = 0, \tag{B17}$$

$$a^2E(a)\tilde{\theta}_d'(a) + (1-3w_d)aE(a)\tilde{\theta}_d(a) + \tilde{k}^2\Phi(a) - \left(\frac{w_d}{1+w_d}\right)\tilde{k}^2\delta_d(a) = 0, \tag{B18}$$

$$\tilde{k}^2\Phi(a) + 3a^2E^2(a)[a\Phi'(a) + \Phi(a)] = \frac{3}{2}a^2[\tilde{\rho}_d(a)\delta_d(a) + \tilde{\rho}_1(a)\delta_1(a) + \tilde{\rho}_2(a)\delta_2(a)]. \tag{B19}$$

Here, $E(a) \equiv H(a)/H_i$, $\tilde{k} \equiv k/H_i$, $\tilde{\theta} \equiv \theta/H_i$, $\tilde{\rho} \equiv \rho/\rho_{{\rm crit},i}$, and a prime denotes a derivative with respect to scale factor, a. Equation (B19) is the perturbed time-time component of the Einstein equation.

We assume perturbations evolve from an initial scale factor of $a_i = 1$ and that the initial time is set sufficiently early such that all modes of interest are superhorizon ($\tilde{k} < 1$). In conformal Newtonian gauge, perturbations are constant outside the horizon at zeroth order in k/aH so we begin by setting $\Phi' = 0$. If ρ_d dominates the energy density of the Universe, then $E(a) \approx a^{-\frac{3}{2}(1+w_d)}$ and $\tilde{\rho}_d(a) \approx a^{-3(1+w_d)}$ because $\rho_{d,i}/\rho_{\mathrm{crit},i} \approx 1$. Under these conditions and dropping terms proportional to $\tilde{k}^2$ and Φ', Eq. (B19) results in $\delta_d(a_i) = 2\Phi(a_i)$ at zeroth order in k/aH. This result can then be used to simplify Eq. (B18), which has the solution

$$\tilde{\theta}_d = -\frac{2a^{\frac{1}{2}(1+3w_d)}}{3(1+w_d)}\tilde{k}^2\Phi_p, \tag{B20}$$

where $\Phi_p \equiv \Phi(a_i)$. The superhorizon initial conditions for δ_1 and δ_2 at zeroth order in k/aH can be found by combining Eqs. (B13), (B15), and (B17) while neglecting $\tilde{\theta} \propto \tilde{k}^2$ terms. In doing so, we find that $\delta_1 = 2\Phi_p(1+w_1)/(1+w_d)$ and $\delta_2 = 2\Phi_p(1+w_2)/(1+w_d)$. Combining these results with Eqs. (B14) and (B16) and solving, it follows that $\tilde{\theta}_d = \tilde{\theta}_1 = \tilde{\theta}_2$. This result is a manifestation of the fact that adiabatic initial conditions in conformal Newtonian gauge have the same velocity perturbations between all fluids [60].

While $\Phi' = 0$ at zeroth order in k/aH, Φ can evolve at higher orders in k/aH. To determine this evolution, we begin by simplifying Eq. (B19) to

$$\frac{1}{3}a^{1-3w_d}\tilde{k}^2\Phi(a) + a\Phi'(a) + \Phi(a) = \frac{1}{2}\delta_d. \tag{B21}$$

Differentiating Eq. (B21) with respect to scale factor and combining with Eqs. (B17) and (B20), we obtain the differential equation

$$0 = a\Phi''(a) + \Phi'(a)\left[\frac{1}{3}a^{1+3w_d}\tilde{k}^2 + \frac{3}{2}(1+w_d) + 2\right] + \Phi(a)[w_d a^{3w_d}\tilde{k}^2]. \tag{B22}$$

Solving Eq. (B22) with the ansatz of $\Phi(\tau) = A + Bk^2\tau^2$, where

$$\tau = \left(\frac{2}{1+3w_d}\right)\frac{a^{\frac{1}{2}(1+3w_d)}}{H_i} \tag{B23}$$

results in

$$\Phi = \Phi_p - \left[\frac{2w_d a^{1+3w_d}}{4-24(1+w_d)+27(1+w_d)^2}\right]\tilde{k}^2\Phi_p + \mathcal{O}(\tilde{k}^3). \tag{B24}$$

Combining Eqs. (B20) and (B24) with either Eqs. (B13), (B15), or (B17), it follows that the adiabatic initial condition for each of the three fluids takes the form of

$$\delta_j \simeq 2\left(\frac{1+w_j}{1+w_d}\right)\Phi_p + \frac{2}{3}\left(\frac{1+w_j}{1+w_d}\right)\left[\frac{7+18w_d+9w_d^2}{7+30w_d+27w_d^2}\right]a^{(1+3w_d)}\tilde{k}^2\Phi_p. \tag{B25}$$

Or, applying the transformation of Eq. (B23),

$$\delta_j \simeq 2\left(\frac{1+w_j}{1+w_d}\right)\Phi_p + \frac{2}{3}\left(\frac{1+w_j}{1+w_d}\right)\left[\frac{7+39w_d+63w_d^2+27w_d^3}{28+36w_d}\right](k\tau)^2\Phi_p. \tag{B26}$$

Note that the term in square brackets is only dependent on w_d and is therefore the same between all individual fluids. Even at next-to-leading order in $k\tau$, the ratio of initial conditions between any two noninteracting fluids is $\delta_i/\delta_j = (1+w_i)/(1+w_j)$.

3. Generalized initial conditions for interacting case

Here we employ a similar approach to that used in Appendix B 2 in order to derive the superhorizon adiabatic initial conditions for interacting fluids in conformal Newtonian gauge. Let us consider three fluids with energy densities ρ_1, ρ_2, and ρ_d, where ρ_d dominates the energy density of the Universe and species 1 is a massive particle ($w_1 = 0$) that decays into species 2 with a decay rate Γ. Equations (16)–(18) describe the energy density evolution of the three species. Each species is assumed to be a perfect fluid with an energy momentum tensor given by Eq. (B9), and so the covariant form of Eqs. (16)–(18) can be written as

$$\nabla_\mu({}^{(i)}T^\mu_\nu) = Q^{(i)}_\nu, \tag{B27}$$

where i specifies each fluid. It follows from Eqs. (16)–(18) that

$$Q^{(d)}_\nu = 0, \tag{B28}$$

$$Q^{(1)}_\nu = {}^{(i)}T_{\mu\nu}u^\mu_{(1)}\Gamma, \tag{B29}$$

$$Q^{(2)}_\nu = -Q^{(1)}_\nu. \tag{B30}$$

We derive the perturbation equations by evaluating Eq. (B27) with the perturbed conformal Newtonian metric

of Eq. (5) and enforcing the same perturbations to the fluid energy density and velocity as in Appendix B 2: $\rho_i(t,\vec{x}) = \rho_i^0(t)[1+\delta_i(t,\vec{x})]$, $u^0 = (1-\Psi)$, and $u^j_{(i)} = (1-\Psi)V^j_{(i)}$. From these perturbations, we find

$$Q_0^{(1)} = \Gamma\rho_1^0(1+\delta_1+\Psi), \tag{B31}$$

$$Q_j^{(1)} = -\Gamma\rho_1^0 a^2\delta_{kj}V_1^k. \tag{B32}$$

Here, the quantity $Q_0^{(1)}$ is composed of a zeroth-order piece, $Q_0^{(1),(0)} \equiv \Gamma\rho_1^0$, and a first order component, $Q_0^{(1),(1)} \equiv \Gamma\rho_1^0(\delta_1+\Psi)$. It follows that the $\nu = 0$ component of Eq. (B27) lends

$$\frac{\mathrm{d}\delta_i}{\mathrm{d}t} + (1+w_i)\frac{\theta_i}{a} + 3(1+w_i)\frac{\mathrm{d}\Phi}{\mathrm{d}t} = \frac{1}{\rho_i^0}\left[Q_0^{(i),(0)}\delta_i - Q_0^{(i),(1)}\right], \tag{B33}$$

and the divergence of the $\nu = j$ component of Eq. (B27) results in

$$\frac{\mathrm{d}\theta_i}{\mathrm{d}t} + (1-3w_i)H\theta_i + \frac{\nabla^2\Psi}{a} + \frac{w_i}{1+w_i}\frac{\nabla^2\delta_i}{a} = \frac{1}{\rho_i^0}\left[\frac{\partial_j Q_j^{(i)}}{a(1+w_i)} + Q_0^{(i),(0)}\theta_i\right]. \tag{B34}$$

Considering the energy exchange between each species described by Eqs. (B28)–(B30), the suite of equations that derive from Eqs. (B33) and (B34) are

$$a^2E(a)\delta_1'(a) + \tilde{\theta}_1(a) + 3a^2E(a)\Phi'(a) = a\tilde{\Gamma}\Phi(a), \tag{B35}$$

$$a^2E(a)\tilde{\theta}_1'(a) + aE(a)\tilde{\theta}_1(a) + \tilde{k}^2\Phi(a) = 0, \tag{B36}$$

$$a^2E(a)\delta_2'(a) + (1+w_2)\tilde{\theta}_2(a) + 3(1+w_2)a^2E(a)\Phi'(a) = a\tilde{\Gamma}\frac{\tilde{\rho}_1(a)}{\tilde{\rho}_2(a)}[\delta_1(a) - \delta_2(a) - \Phi(a)], \tag{B37}$$

$$a^2E(a)\tilde{\theta}_2'(a) + (1-3w_2)aE(a)\tilde{\theta}_2(a) + \tilde{k}^2\Phi(a) - \left(\frac{w_2}{1+w_2}\right)\tilde{k}^2\delta_2(a) = a\tilde{\Gamma}\frac{\tilde{\rho}_1(a)}{\tilde{\rho}_2(a)}\left[\frac{\tilde{\theta}_1(a)}{1+w_2} - \tilde{\theta}_2(a)\right], \tag{B38}$$

$$a^2E(a)\delta_d'(a) + (1+w_d)\tilde{\theta}_d(a) + 3(1+w_d)a^2E(a)\Phi'(a) = 0, \tag{B39}$$

$$a^2E(a)\tilde{\theta}_d'(a) + (1-3w_d)aE(a)\tilde{\theta}_d(a) + \tilde{k}^2\Phi(a) - \left(\frac{w_d}{1+w_d}\right)\tilde{k}^2\delta_d(a) = 0, \tag{B40}$$

$$\tilde{k}^2\Phi(a) + 3a^2E^2(a)[a\Phi'(a) + \Phi(a)] = \frac{3}{2}a^2[\tilde{\rho}_d(a)\delta_d(a) + \tilde{\rho}_1(a)\delta_1(a) + \tilde{\rho}_2(a)\delta_2(a)]. \tag{B41}$$

Here, $\tilde{\Gamma} \equiv \Gamma/H_i$ and again Eq. (B41) is the perturbed time-time Einstein equation.

At zeroth order in k/aH, $\Phi' = 0$ outside the horizon in conformal Newtonian gauge. As in Appendix B 2, we assume $\tilde{\rho}_d \gg \tilde{\rho}_1, \tilde{\rho}_2$ such that $E(a) \approx a^{-\frac{3}{2}(1+w_d)}$ and $\tilde{\rho}_d(a) \approx a^{-3(1+w_d)}$. Applying the superhorizon limit $(\tilde{k}^2, \Phi' \to 0)$ to Eq. (B41) results in $\delta_d(a_i) = 2\Phi(a_i)$ at zeroth order in k/aH. This solution can be combined with Eq. (B40) which results in $\tilde{\theta}_d$ being equivalent to Eq. (B20). The initial condition at zeroth order in k/aH for δ_1 can be derived by combining Eqs. (B35) and (B39) and dropping $\tilde{\theta} \propto \tilde{k}^2$ terms. Additionally, we assume that the initial time is set sufficiently early such that Γ/H_i is initially small. This leads to $\delta_1 = 2\Phi_p/(1+w_d)$ at zeroth order in k/aH, which mirrors the noninteracting case of Appendix B 2 since $w_1 = 0$. To solve for the initial condition of δ_2 at zeroth order in k/aH, we combine the zeroth-order result for δ_1 with Eq. (B37) while neglecting any $\tilde{\theta} \propto \tilde{k}^2$ terms, and enforcing that $\delta_2' = \Phi' = 0$ on superhorizon scales. Doing so results in $\delta_2 = \Phi_p[(1-w_d)/(1+w_d)]$ at zeroth order in k/aH. Inserting these zeroth-order results for δ_1 and δ_2 in Eqs. (B36) and (B38) leads to $\tilde{\theta}_1 = \tilde{\theta}_2 = \tilde{\theta}_d$ all being equivalent to Eq. (B20). This confirms that, even in the presence of energy transfer, the initial velocity perturbation for all fluids is universal for adiabatic perturbations in conformal Newtonian gauge.

Since the evolution of $\Phi(a)$ on superhorizon scales is completely determined by the dominant species of the

Universe, and ρ_d is still noninteracting, it follows that the superhorizon evolution of $\Phi(a)$ at second order in k/aH is still given by Eq. (B24). This would still be true if ρ_1 were the dominant energy density instead of ρ_d; even though species 1 is interacting, the evolution of ρ_1 is unaffected by this interaction and so its influence on $\Phi(a)$ is equivalent to that of a noninteracting dominant fluid.

Equipped with $\tilde{\theta}(a)$ and $\Phi(a)$ at second order in k/aH, we can derive the adiabatic initial conditions for δ_1, δ_2, and δ_d at order $(k/aH)^2$. Combining Eqs. (B20) and (B24) with either Eq. (B35) or Eq. (B39), and applying Eq. (B23) to report in terms of τ, the density perturbations for species 1 is

$$\delta_1 \simeq 2\left(\frac{1}{1+w_d}\right)\Phi_p + \frac{2}{3}\left(\frac{1}{1+w_d}\right)\left[\frac{7+39w_d+63w_d^2+27w_d^3}{28+36w_d}\right](k\tau)^2\Phi_p, \tag{B42}$$

and the density perturbation for the dominant species is

$$\delta_d \simeq 2\Phi_p + \frac{2}{3}\left[\frac{7+39w_d+63w_d^2+27w_d^3}{28+36w_d}\right](k\tau)^2\Phi_p. \tag{B43}$$

Both Eqs. (B42) and (B43) are equivalent to Eq. (B26) in Appendix B 2 (since $w_1 = 0$). For species 2, inserting Eqs. (B20) and (B24) into Eq. (B37) and applying the transformation Eq. (B23) results in

$$\delta_2 \simeq \left(\frac{1-w_d}{1+w_d}\right)\Phi_p + \mathcal{W}(k\tau)^2\Phi_p, \tag{B44}$$

where $\mathcal{W}$ is a constant equal to

$$\mathcal{W} = \frac{1+3w_d}{6(5+6w_2+9w_d)(7+16w_d+9w_d^2)} \times [35+162w_d+225w_d^2+90w_d^3 + 2w_2(28+102w_d+99w_d^2+27w_d^3)]. \tag{B45}$$

APPENDIX C: POSTDECAY $N_{\rm eff}$

Decays in the short-lived regime are primarily constrained by their influence on the CMB anisotropies via changes in $\Delta N_{\rm eff}$ from injected DR. Here, we derive a mapping between the $\Delta N_{\rm eff}$ resulting from a decay and the decay parameters R_Γ and Γ_Y.

Let us define the ratio of the comoving radiation energy density before and after the decay as

$$g \equiv \frac{(\rho_{sr,f}+\rho_{{\rm dr},f})a_f^4}{\rho_{sr,i}a_i^4}, \tag{C1}$$

where ρ_{sr} is the combined radiation energy density of photons and massless neutrinos, $\rho_{\rm dr}$ is the energy density of DR, and the i and f subscripts denote before and after significant production of DR from the decay, respectively. To fit g as a function of R_Γ and Γ_Y, we apply the sudden decay approximation in which all of the Y particle's energy is instantaneously converted to DR at a scale factor of $a_{\rm SD}$. Under this approximation, we have

$$g-1 = \frac{\rho_{sr,f}a_f^4+\rho_{{\rm dr},f}a_f^4-\rho_{sr,i}a_i^4}{\rho_{sr,i}a_i^4} \approx \frac{\rho_{\rm dr}(a_{\rm SD})}{\rho_{sr}(a_{\rm SD})}, \tag{C2}$$

where we have assumed that the standard comoving radiation is unchanged (i.e. $\rho_{sr,i}a_i^4 = \rho_{sr,f}a_f^4$) and that the decay is instantaneous such that $a_i = a_f = a_{\rm SD}$. Taking $\rho_{\rm dr}(a_{\rm SD}) = \rho_Y(a_{\rm SD})$, it follows that

$$g-1 \approx \left(\frac{a_{\rm SD}}{a_i}\right)\frac{\rho_{Y,i}}{\rho_{sr,i}} \approx \left(\frac{a_{\rm SD}}{a_i}\right)\frac{\rho_{Y,i}}{\rho_{r,i}}\epsilon^{-1}, \tag{C3}$$

where $\epsilon \equiv \rho_{sr,i}/\rho_{r,i}$ and $\rho_{r,i} = \rho_{sr,i}+\rho_{{\rm ncdm},i}$. Inserting Eq. (A2) into Eq. (C3) gives

$$\frac{g-1}{R_\Gamma \xi} \approx \frac{a_{\rm SD}}{a_\Gamma}, \tag{C4}$$

where

$$\xi = \frac{1}{\epsilon}\times\begin{cases}\left(1+\frac{a_\Gamma}{a_i}\frac{\rho_{sm,i}}{\rho_{r,i}}\right), & a_\Gamma < a_p \\ \left[\epsilon+\frac{a_\Gamma}{a_i}\frac{\rho_{sm,i}}{\rho_{r,i}}+(1-\epsilon)\left(\frac{a_i}{a_p}\right)\frac{a_\Gamma}{a_i}\right], & a_\Gamma > a_p\end{cases}. \tag{C5}$$

Both $a_{\rm SD}$ and a_Γ parametrize the scale factor at which $\Gamma_Y \approx H$, so we expect these quantities to be similar in all decay scenarios. The left-hand side of Eq. (C4) should therefore have a simple functional form that minimally depends on R_Γ and Γ_Y. Figure 11 shows $(g-1)/(R_\Gamma\xi)$ as a function of R_Γ and Γ_Y. Here we see a plateau at large Γ_Y, corresponding to cases in which the Y particle decays deep in radiation domination, and another plateau at smaller Γ_Y corresponding to scenarios in which the decay predominately occurs during matter domination.

The small dependencies that $(g-1)/(R_\Gamma\xi)$ has on R_Γ and Γ_Y in Fig. 11 are the result of inaccuracies in the sudden decay approximation, which incorrectly assumes the decay to be instantaneous. While the duration of the decay depends on proper time, t, the amount that ρ_Y changes while $\rho_{\rm dr}$ is being produced is dependent on scale factor. Therefore, the height of the plateaus change depending on if the decay occurs predominately in radiation or matter domination because the mapping between t and a is different for these two regimes. At large Γ_Y, there is a slight dependence on R_Γ because an increase in R_Γ leads to a larger contribution of ρ_Y and thus a deviation from radiation domination. Towards smaller Γ_Y the dependence

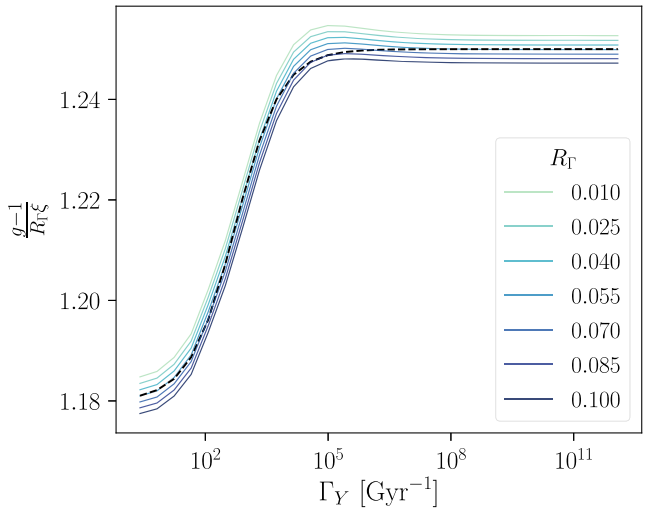

FIG. 11. Dependence of Eq. (C4) as a function of both R_Γ and Γ_Y. Deep in radiation domination (large Γ_Y), this quantity has no dependence on Γ_Y and only a minimal dependence on R_Γ. The dashed black line shows the numerical fit of Eq. (C6).

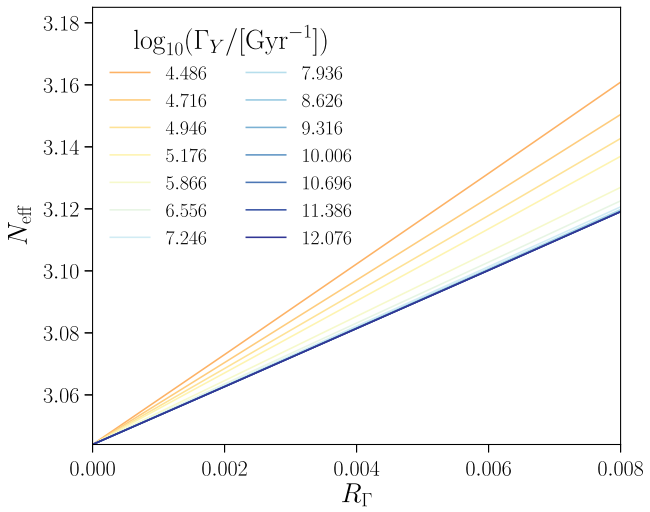

FIG. 12. Postdecay N_{eff} for varying values of R_Γ and Γ_Y. For short-lived cases in which the Y particle decays during radiation domination, ΔN_{eff} is simply a function of R_Γ. Once the energy density of nonrelativistic matter begins making a non-negligible contribution to the total energy density, ΔN_{eff} also becomes sensitive to Γ_Y.

on R_Γ stems from a deviation from matter domination; an increase in R_Γ leads to more DR production and a further deviation from matter domination.

The dashed black line in Fig. 11 shows a numerical fit described by

$$\frac{g-1}{R_\Gamma \xi} = \frac{x + y(x^{-1}\Gamma_Y)^z}{1 + (x^{-1}\Gamma_Y)^z}, \tag{C6}$$

for $x = 1.18$, $y = 1.25$, and $z = 0.78$. From this fit, we can determine $g(R_\Gamma, \Gamma_Y)$. If N_{ur} is the effective number of relativistic species before injection, excluding the massive neutrino, and N'_{ur} is the corresponding number after the injection of DR, then it follows that

$$g = \frac{(\rho_{sr,f} + \rho_{\mathrm{dr},f})a_f^4}{\rho_{sr,i}a_i^4} = \frac{\rho_{\gamma,f}a_f^4\left[1 + \frac{7}{8}N'_{ur}\left(\frac{4}{11}\right)^{4/3}\right]}{\rho_{\gamma,i}a_i^4\left[1 + \frac{7}{8}N_{ur}\left(\frac{4}{11}\right)^{4/3}\right]}. \tag{C7}$$

The comoving photon energy density does not change and so this reduces to

$$N'_{ur} = N_{ur} + (g-1)\left[\frac{8}{7}\left(\frac{11}{4}\right)^{4/3} + N_{ur}\right]. \tag{C8}$$

The contribution that the single massive neutrino species makes to N_{eff} is $N_{\mathrm{ncdm}} = (11/4)^{4/3}(0.71611)^4 = 1.0132$, and we enforce that $N_{\mathrm{eff}} = N_{ur} + N_{\mathrm{ncdm}}$ is equal to 3.044 before the injection of any DR. The postdecay N_{eff} is then determined via Eq. (C8). Figure 12 shows the postdecay N_{eff} values for a range of R_Γ and Γ_Y. For a fixed Γ_Y, a larger R_Γ corresponds to larger ΔN_{eff}, as expected. If a decay scenario occurs deep in radiation domination, then ΔN_{eff} is solely a function of R_Γ. However, as we approach Y particle lifetimes that extend to matter domination, ΔN_{eff} picks up an additional dependence on Γ_Y. This dependence on Γ_Y stems from how R_Γ is defined. R_Γ is a measure of the energy density of the Y particle compared to the total energy density of the Universe at the scale factor of a_Γ. In other words, $R_\Gamma \sim \rho_Y(a_\Gamma)/\rho_d(a_\Gamma) \sim \rho_{\mathrm{dr}}(a_\Gamma)/\rho_d(a_\Gamma)$, where ρ_d is the dominant species. Therefore, if $a_\Gamma \ll a_{\mathrm{eq}}$, $R_\Gamma \sim \rho_{\mathrm{dr}}(a_\Gamma)/\rho_{sr}(a_\Gamma)$ and thus ΔN_{eff} is solely dependent on R_Γ. However, if $a_\Gamma > a_{eq}$, then $R_\Gamma \sim \rho_{\mathrm{dr}}(a_\Gamma)/\rho_m(a_\Gamma) \sim [\rho_{\mathrm{dr}}(a_\Gamma)/\rho_{sr}(a_\Gamma)] \times [\rho_{sr}(a_\Gamma)/\rho_m(a_\Gamma)]$ and so $\Delta N_{\mathrm{eff}} \sim R_\Gamma \times [\rho_m(a_\Gamma)/\rho_{sr}(a_\Gamma)]$ for Y particle lifetimes extending into matter domination.

[1] N. Aghanim *et al.* (Planck Collaboration), Astron. Astrophys. **641**, A6 (2020).
[2] S. Alam, M. Ata, S. Bailey, F. Beutler, D. Bizyaev, J. A. Blazek, A. S. Bolton, J. R. Brownstein, A. Burden, C.-H. Chuang *et al.*, Mon. Not. R. Astron. Soc. **470**, 2617 (2017).
[3] S. Alam *et al.* (eBOSS Collaboration), Phys. Rev. D **103**, 083533 (2021).
[4] C. Heymans, T. Tröster, M. Asgari, C. Blake, H. Hildebrandt, B. Joachimi, K. Kuijken, C.-A. Lin, A. G. Sánchez, J. L. van den Busch *et al.*, Astron. Astrophys. **646**, A140 (2021).
[5] T. M. C. Abbott *et al.* (DES Collaboration), Phys. Rev. D **105**, 023520 (2022).
[6] W. Yuan, A. G. Riess, L. M. Macri, S. Casertano, and D. Scolnic, Astrophys. J. **886**, 61 (2019).
[7] K. C. Wong, S. H. Suyu, G. C.-F. Chen, C. E. Rusu, M. Millon, D. Sluse, V. Bonvin, C. D. Fassnacht, S. Taubenberger, M. W. Auger *et al.*, Mon. Not. R. Astron. Soc. **498**, 1420 (2020).
[8] J. P. Blakeslee, J. B. Jensen, C.-P. Ma, P. A. Milne, and J. E. Greene, Astrophys. J. **911**, 65 (2021).
[9] A. G. Riess, W. Yuan, L. M. Macri, D. Scolnic, D. Brout, S. Casertano, D. O. Jones, Y. Murakami, L. Breuval, T. G. Brink *et al.*, Astrophys. J. Lett. **934**, L7 (2022).
[10] T. M. C. Abbott *et al.* (DES Collaboration), Open J. Astrophys. **6** (2023), 10.21105/astro.2305.17173.
[11] G. Efstathiou, Mon. Not. R. Astron. Soc. **440**, 1138 (2014).
[12] G. E. Addison, Y. Huang, D. J. Watts, C. L. Bennett, M. Halpern, G. Hinshaw, and J. L. Weiland, Astrophys. J. **818**, 132 (2016).
[13] N. Aghanim *et al.* (Planck Collaboration), Astron. Astrophys. **607**, A95 (2017).
[14] K. Aylor, M. Joy, L. Knox, M. Millea, S. Raghunathan, and W. L. K. Wu, Astrophys. J. **874**, 4 (2019).
[15] T. Shanks, L. Hogarth, and N. Metcalfe, Mon. Not. R. Astron. Soc. **484**, L64 (2019).
[16] J. Soltis, A. Farahi, D. Huterer, and C. M. Liberato II, Phys. Rev. Lett. **122**, 091301 (2019).
[17] A. G. Riess, G. S. Anand, W. Yuan, S. Casertano, A. Dolphin, L. M. Macri, L. Breuval, D. Scolnic, M. Perrin, and R. I. Anderson, Astrophys. J. Lett. **956**, L18 (2023).
[18] T. Karwal and M. Kamionkowski, Phys. Rev. D **94**, 103523 (2016).
[19] V. Poulin, T. L. Smith, T. Karwal, and M. Kamionkowski, Phys. Rev. Lett. **122**, 221301 (2019).
[20] T. L. Smith, V. Poulin, and M. A. Amin, Phys. Rev. D **101**, 063523 (2020).
[21] R. Murgia, G. F. Abellán, and V. Poulin, Phys. Rev. D **103**, 063502 (2021).
[22] J. L. Bernal, L. Verde, and A. G. Riess, J. Cosmol. Astropart. Phys. 10 (2016) 019.
[23] E. Di Valentino, A. Melchiorri, and J. Silk, J. Cosmol. Astropart. Phys. 01 (2020) 013.
[24] V. Simha and G. Steigman, J. Cosmol. Astropart. Phys. 06 (2008) 016.
[25] M. Hufnagel, K. Schmidt-Hoberg, and S. Wild, J. Cosmol. Astropart. Phys. 02 (2018) 044.
[26] A. Berlin, N. Blinov, and S. W. Li, Phys. Rev. D **100**, 015038 (2019).
[27] R. An and V. Gluscevic, Phys. Rev. D **109**, 023534 (2024).
[28] D. Aloni, M. Joseph, M. Schmaltz, and N. Weiner, Phys. Rev. Lett. **131**, 221001 (2023).
[29] S. Bashinsky and U. Seljak, Phys. Rev. D **69**, 083002 (2004).
[30] Z. Hou, R. Keisler, L. Knox, M. Millea, and C. Reichardt, Phys. Rev. D **87**, 083008 (2013).
[31] B. Follin, L. Knox, M. Millea, and Z. Pan, Phys. Rev. Lett. **115**, 091301 (2015).
[32] K. Vattis, S. M. Koushiappas, and A. Loeb, Phys. Rev. D **99**, 121302 (2019).
[33] S. J. Clark, K. Vattis, and S. M. Koushiappas, Phys. Rev. D **103**, 043014 (2021).
[34] F. McCarthy and J. C. Hill, Phys. Rev. D **108**, 063501 (2023).
[35] A. C. Sobotka, A. L. Erickcek, and T. L. Smith, Phys. Rev. D **107**, 023525 (2023).
[36] V. Poulin and P. D. Serpico, Phys. Rev. D **91**, 103007 (2015).
[37] V. Poulin, J. Lesgourgues, and P. D. Serpico, J. Cosmol. Astropart. Phys. 03 (2017) 043.
[38] M. Kawasaki, K. Kohri, T. Moroi, and Y. Takaesu, Phys. Rev. D **97**, 023502 (2018).
[39] M. Hufnagel, K. Schmidt-Hoberg, and S. Wild, J. Cosmol. Astropart. Phys. 11 (2018) 032.
[40] L. Forestell, D. E. Morrissey, and G. White, J. High Energy Phys. 01 (2019) 74.
[41] M. Kawasaki, K. Kohri, T. Moroi, K. Murai, and H. Murayama, J. Cosmol. Astropart. Phys. 12 (2020) 048.
[42] C. Balázs, S. Bloor, T. E. Gonzalo, W. Handley, S. Hoof, F. Kahlhoefer, M. Lecroq, D. J. E. Marsh, J. J. Renk, P. Scott *et al.*, J. Cosmol. Astropart. Phys. 12 (2022) 027.
[43] J. C. Mather, E. S. Cheng, D. A. Cottingham, R. E. Eplee, Jr., D. J. Fixsen, T. Hewagama, R. B. Isaacman, K. A. Jensen, S. S. Meyer, P. D. Noerdlinger *et al.*, Astrophys. J. **420**, 439 (1994).
[44] D. J. Fixsen, E. S. Cheng, J. M. Gales, J. C. Mather, R. A. Shafer, and E. L. Wright, Astrophys. J. **473**, 576 (1996).
[45] A. Kogut, D. J. Fixsen, D. T. Chuss, J. Dotson, E. Dwek, M. Halpern, G. F. Hinshaw, S. M. Meyer, S. H. Moseley, M. D. Seiffert, D. N. Spergel, and E. J. Wollack, J. Cosmol. Astropart. Phys. 07 (2011) 025.
[46] J. Chluba, Mon. Not. R. Astron. Soc. **454**, 4182 (2015).
[47] B. Bolliet, J. Chluba, and R. Battye, Mon. Not. R. Astron. Soc. **507**, 3148 (2021).
[48] J. Chluba, M. H. Abitbol, N. Aghanim, Y. Ali-Haimoud, M. Alvarez, K. Basu, B. Bolliet, C. Burigana, P. de Bernardis, J. Delabrouille *et al.*, Exp. Astron. **51**, 1515 (2021).
[49] K. Ichiki, M. Oguri, and K. Takahashi, Phys. Rev. Lett. **93**, 071302 (2004).
[50] B. Audren, J. Lesgourgues, G. Mangano, P. D. Serpico, and T. Tram, J. Cosmol. Astropart. Phys. 12 (2014) 028.
[51] V. Poulin, P. D. Serpico, and J. Lesgourgues, J. Cosmol. Astropart. Phys. 08 (2016) 036.
[52] L. Xiao, L. Zhang, R. An, C. Feng, and B. Wang, J. Cosmol. Astropart. Phys. 01 (2020) 045.
[53] A. Nygaard, T. Tram, and S. Hannestad, J. Cosmol. Astropart. Phys. 05 (2021) 017.
[54] S. Alvi, T. Brinckmann, M. Gerbino, M. Lattanzi, and L. Pagano, J. Cosmol. Astropart. Phys. 11 (2022) 015.

[55] J. Bucko, S. K. Giri, and A. Schneider, Astron. Astrophys. **672**, A157 (2023).
[56] R. Chown, Y. Omori, K. Aylor, B. A. Benson, L. E. Bleem, J. E. Carlstrom, C. L. Chang, H.-M. Cho, T. Crawford, A. T. Crites *et al.*, Astrophys. J. Suppl. Ser. **239**, 10 (2018).
[57] D. Dutcher, L. Balkenhol, P. A. R. Ade, Z. Ahmed, E. Anderes, A. J. Anderson, M. Archipley, J. S. Avva, K. Aylor, P. S. Barry *et al.*, Phys. Rev. D **104**, 022003 (2021).
[58] L. Balkenhol, D. Dutcher, A. S. Mancini, A. Doussot, K. Benabed, S. Galli, P. A. R. Ade, A. J. Anderson, B. Ansarinejad, M. Archipley *et al.*, Phys. Rev. D **108**, 023510 (2023).
[59] D. Scolnic, D. Brout, A. Carr, A. G. Riess, T. M. Davis, A. Dwomoh, D. O. Jones, N. Ali, P. Charvu, R. Chen *et al.*, Astrophys. J. **938**, 113 (2022).
[60] C.-P. Ma and E. Bertschinger, Astrophys. J. **455**, 7 (1995).
[61] D. Blas, J. Lesgourgues, and T. Tram, J. Cosmol. Astropart. Phys. 07 (2011) 034.
[62] A. L. Erickcek, P. Ralegankar, and J. Shelton, J. Cosmol. Astropart. Phys. 01 (2022) 017.
[63] S. Weinberg, Phys. Rev. D **67**, 123504 (2003).
[64] G. Ballesteros and J. Lesgourgues, J. Cosmol. Astropart. Phys. 10 (2010) 014.
[65] E. B. Holm, L. Herold, S. Hannestad, A. Nygaard, and T. Tram, Phys. Rev. D **107**, L021303 (2023).
[66] J. A. Kable, G. E. Addison, and C. L. Bennett, Astrophys. J. **905**, 164 (2020).
[67] S. Vagnozzi, Phys. Rev. D **104**, 063524 (2021).
[68] D. Baumann, D. Green, J. Meyers, and B. Wallisch, J. Cosmol. Astropart. Phys. 01 (2016) 007.
[69] S. Gariazzo, P. F. de Salas, O. Pisanti, and R. Consiglio, Comput. Phys. Commun. **271**, 108205 (2022).
[70] D. Aloni, A. Berlin, M. Joseph, M. Schmaltz, and N. Weiner, Phys. Rev. D **105**, 123516 (2022).
[71] K. L. Pandey, T. Karwal, and S. Das, J. Cosmol. Astropart. Phys. 07 (2020) 026.
[72] B. Audren, J. Lesgourgues, K. Benabed, and S. Prunet, J. Cosmol. Astropart. Phys. 02 (2013) 001.
[73] T. Brinckmann and J. Lesgourgues, Phys. Dark Universe **24**, 100260 (2019).
[74] W. Lin, X. Chen, and K. J. Mack, Astrophys. J. **920**, 159 (2021).
[75] D. Brout, D. Scolnic, B. Popovic, A. G. Riess, J. Zuntz, R. Kessler, A. Carr, T. M. Davis, S. Hinton, D. Jones *et al.*, Astrophys. J. **938**, 110 (2022).
[76] R. Cooke, M. Pettini, and C. C. Steidel, Astrophys. J. **855**, 102 (2018).
[77] A. Gelman and D. B. Rubin, Stat. Sci. **7**, 457 (1992).
[78] A. Lewis, arXiv:1910.13970.
[79] N. Aghanim *et al.* (Planck Collaboration), Astron. Astrophys. **641**, A8 (2020).
[80] F. Beutler, C. Blake, M. Colless, D. H. Jones, L. Staveley-Smith, L. Campbell, Q. Parker, W. Saunders, and F. Watson, Mon. Not. R. Astron. Soc. **416**, 3017 (2011).
[81] A. J. Ross, L. Samushia, C. Howlett, W. J. Percival, A. Burden, and M. Manera, Mon. Not. R. Astron. Soc. **449**, 835 (2015).
[82] D. M. Scolnic, D. O. Jones, A. Rest, Y. C. Pan, R. Chornock, R. J. Foley, M. E. Huber, R. Kessler, G. Narayan, A. G. Riess *et al.*, Astrophys. J. **859**, 101 (2018).
[83] S. J. Clark, K. Vattis, J. Fan, and S. M. Koushiappas, Phys. Rev. D **107**, 083527 (2023).
[84] K. Jedamzik, L. Pogosian, and G.-B. Zhao, Commun. Phys. **4**, 123 (2021).
[85] S. Vagnozzi, Universe **9**, 393 (2023).
[86] N. Schöneberg, G. F. Abellán, A. P. Sánchez, S. J. Witte, V. Poulin, and J. Lesgourgues, Phys. Rep. **984**, 1 (2022).
[87] V. Poulin, T. L. Smith, and T. Karwal, Phys. Dark Universe **42**, 101348 (2023).
[88] M. Joseph, D. Aloni, M. Schmaltz, E. N. Sivarajan, and N. Weiner, Phys. Rev. D **108**, 023520 (2023).
[89] I. J. Allali, M. P. Hertzberg, and F. Rompineve, Phys. Rev. D **104**, L081303 (2021).
[90] J. S. Cruz, F. Niedermann, and M. S. Sloth, J. Cosmol. Astropart. Phys. 11 (2023) 033.
[91] H. Ganjoo, A. L. Erickcek, W. Lin, and K. J. Mack, J. Cosmol. Astropart. Phys. 01 (2023) 004.